The Thesis Committee for Kyung Woo Min
Certifies that this is the approved version of the following thesis:

Applications of Impedance-based Fault Locating Methods in Power Systems

APPROVED BY

SUPERVISING COMMITTEE:

Surya Santoso, Supervisor

Ross Baldick

Applications of Impedance-based Fault Locating Methods in Power Systems

by

Kyung Woo Min, B.S.

THESIS

Presented to the Faculty of the Graduate School of

The University of Texas at Austin

in Partial Fulfillment

of the Requirements

for the Degree of

MASTER OF SCIENCE IN ENGINEERING

THE UNIVERSITY OF TEXAS AT AUSTIN

May 2014

Dedicated to my parents for their love and support.

Acknowledgments

I would like to thank Dr. Santoso, my advisor, for the mindful guidance in completing this work. I would also like to thank Dr. Baldick for reading this thesis.

Applications of Impedance-based Fault Locating Methods in Power Systems

Kyung Woo Min, M.S.E.
The University of Texas at Austin, 2014

Supervisor: Surya Santoso

The concentration of this work is in estimating fault locations in power systems. After describing the basic concepts of fault locating methods, this work describes improving the fault location estimates, applying the fault locating methods, and implementing the methods in a software. Every work described in the Chapter will be evaluated whether by actual field data or simulated data based on field parameters.

Table of Contents

List of Tables

List of Figures

Chapter 1

Introduction

1.1 Motivation

The electric power system delivers electric power produced from generators to loads. The infrastructure is comprised of transmission systems, where the generated electric power is sent to local substations, and distribution systems, where the electric power is delivered to end users from the local substations.

Electric faults happen in both transmission systems and distribution systems. Typical causes of faults are short-circuits involving line(s) and ground, contacts with birds or trees, or lightning events. When a fault occurs in a power line, the protection equipment automatically disconnects the line in order to protect electric devices and to prevent more severe power system failure. Accurate estimation of the fault location is desired to minimize the economic losses due to the failure and to improve power system reliability. Impedance-based fault locating methods are some of the most popular methods used by system operators because they are simple to implement and give reasonable location estimates with high interpretability.

1.2 Objective

The objective of this thesis is to improve the fault location estimates, to evaluate the fault locating methods applied in an actual circuit model, and to implement the fault locating methods in a commercial short-circuit software. The thesis concentrates on using impedance-based methods for locating faults.

First, an overview of impedance-based fault locating methods are briefly summarized in Chapter 2. The methods described in this Chapter will be used as base methods throughout the thesis. Chapters 3 and 4 discuss improving the fault location estimates. Chapter 3 describes improving the location estimates by increasing the accuracy of input phasors of the fault locating methods. In Chapter 4, an approach is suggested to improve the location estimates for a case when distributed generation is connected to a distributed system.

The fault locating methods presented in Chapter 2 are applied and evaluated using simulated fault data in Chapter 5. A time-domain simulation is modeled using actual model parameters and is used to produce fault data needed for the study.

The last Chapter describes implementing the impedance-based fault locating methods in a commercial software. CAPE (Computer-Aided Protection Engineering) software is used as an example program and the fault locating methods are programmed as macros. The macros are developed to be user-friendly with directions guided by graphical interfaces.

Chapter 2

Overview of Impedance-Based Fault Locating Methods

Impedance-based fault locating methods are commonly used in transmission systems and distribution systems to locate faults on the power lines. The methods include the simple reactance, the Takagi, the Novosel, the Eriksson, and the two-ended methods [1–6]. Accurate estimation of the fault location is desired to expedite the service restoration. The basic concept is to utilize voltage and current measurements from intelligent electronic devices (IED), such as digital relays, digital fault recorders and power quality monitors, and estimate the impedance to the fault point from the monitor. Knowing the line impedance per unit distance, the fault location can be estimated by dividing the estimated apparent impedance by the line impedance per unit distance.

Fault locating methods using measurements from a local substation are referred to as one-ended methods while fault locating using measurements from both local and remote ends are referred to as two-ended methods. Two-ended methods generally give more accurate and robust location estimates than one-ended methods and are preferred if the measurements from both ends are

available.

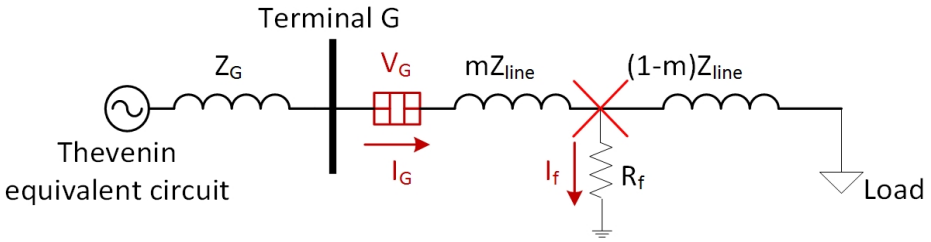

Figure 2.1: One-line Diagram of a Radial System.

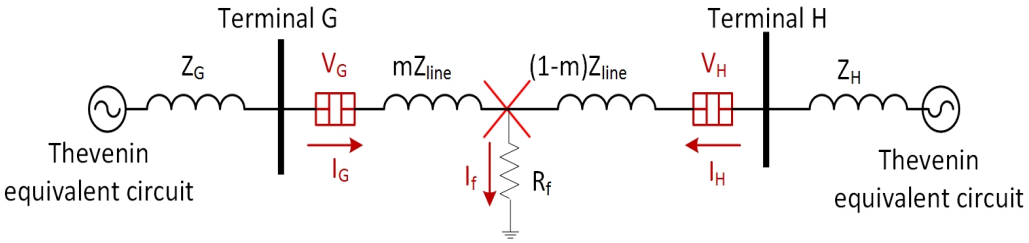

Figure 2.2: One-line Diagram of a Non-Radial System.

2.1 One-ended Impedance-based Methods

One-ended impedance-based methods estimate the fault location by calculating the apparent impedance from voltage and current measurements from one end. Consider a simple one-line diagram of a radial system illustrated in Figure 2.1. The local terminal and the remote terminal are labeled G and H. The voltage drop and the apparent impedance calculated from the monitor

to the faulted point are expressed in Equations 2.1 and 2.2.

$$V_G = mZ_{line,1}I_G + R_f I_f \tag{2.1}$$

$$Z_{app} = \frac{V_G}{I_G} = mZ_{line,1} + R_f \frac{I_f}{I_G} \tag{2.2}$$

For a bolted fault, impedance-based methods give accurate location estimates since the fault resistance R_f in Equation 2.2 is zero. The estimated fault location m is calculated by simply taking the ratio of the apparent impedance to the positive-sequence line impedance $Z_{line,1}$. However, it is unusual to have a bolted fault. The presence of R_f makes the following fault locating methods necessary to reduce the error induced by the fault resistance. Note that the estimated fault locations m in Equations 2.1 and 2.2 are in per-unit. The actual distance can be calculated by multiplying m to the total length of the line.

2.1.1 Simple Reactance Method

The simple reactance method [2] assumes that I_f and I_G expressed in Equation 2.2 are in phase. Based on this assumption, the error term $R_F \frac{I_f}{I_G}$ is assumed to have a real value. As a result, the simple reactance method takes the ratio of the imaginary portion of the apparent impedance to the imaginary portion of the line impedance to calculate the location estimate.

$$m = \frac{imag(\frac{V_G}{I_G})}{imag(Z_{line,1})} \tag{2.3}$$

2.1.2 Takagi Method

The Takagi method [3] utilizes the pre-fault current measurement and takes into account the contribution of load currents in the location estimate. This method assumes that the load current is the same both before and during the fault. By substituting I_f in Equation 2.2 with I_{sup} defined in Equation 2.4, the location estimate given by the Takagi method is derived.

$$I_{sup} = I_G - I_{G,prefault} \tag{2.4}$$

$$m = \frac{imag(V_G I_{sup}^*)}{imag(Z_{line,1} I_G I_{sup}^*)} \tag{2.5}$$

2.1.3 Novosel et al. Method

The Novosel et al. method takes a different approach from the Takagi method by modeling the load as a constant impedance. The method estimates the load impedance from pre-fault current and voltage measurements. The location estimate is calculated by Equation 2.7. Among the two possible estimates of m, the value between 0 and 1 pu should be chosen as the location estimate.

$$Z_{load} = \frac{V_{G,prefault}}{I_{G,prefault}} - Z_{line,1} \tag{2.6}$$

$$m = \frac{(a - \frac{eb}{f}) \pm \sqrt{(a - \frac{eb}{f})^2 - 4(c - \frac{eb}{f})}}{2} \tag{2.7}$$

where the constants are defined as,

$$a + jb = \frac{V_G}{Z_{line1,I_G}} + \frac{Z_{load}}{Z_{line1}} + 1 \tag{2.8}$$

$$c + jd = (\frac{V_G}{Z_{line1,I_G}})(1 + \frac{Z_{load}}{Z_{line1}}) \tag{2.9}$$

$$e + jf = (\frac{I_{sup}}{Z_{line1,I_G}})(1 + \frac{Z_{load} + Z_G}{Z_{line1}}) \tag{2.10}$$

The source impedance Z_G can be estimated using the following equation.

$$Z_G = -\frac{V_G - V_{G,prefault}}{I_G - I_{prefault}} \tag{2.11}$$

2.1.4 Eriksson Method

The Eriksson method takes into account both the load current and the fault current contribution from a remote generation. Therefore, it is applicable when there is an additional generation at the remote end as shown in Figure 2.2. The method uses equivalent source impedance values from both ends of the line (Z_G and Z_H) and takes into account the contribution of the remote infeed fault current. Like the Novosel et al. method the value m is chosen to be the value between 0 and 1 pu.

$$m = \frac{(a - \frac{eb}{f}) \pm \sqrt{(a - \frac{eb}{f})^2 - 4(c - \frac{eb}{f})}}{2} \tag{2.12}$$

where the constants are defined as,

$$a + jb = \frac{V_G}{Z_{line1} I_G} + \frac{Z_H}{Z_{line1}} + 1 \tag{2.13}$$

$$c + jd = (\frac{V_G}{Z_{line1} I_G})(1 + \frac{Z_H}{Z_{line1}}) \tag{2.14}$$

$$e + jf = (\frac{I_{sup}}{Z_{line1} I_G})(1 + \frac{Z_H + Z_G}{Z_{line1}}) \tag{2.15}$$

Table 2.1: Modification of I_G and V_G for unbalanced faults

Type	I_G	V_G
Single line-to-ground (A-G)	$I_{GA} + (\frac{Z_{line,0}}{Z_{line,1}} - 1)I_{G0}$	V_{GA}
Single line-to-ground (B-G)	$I_{GB} + (\frac{Z_{line,0}}{Z_{line,1}} - 1)I_{G0}$	V_{GB}
Single line-to-ground (C-G)	$I_{GC} + (\frac{Z_{line,0}}{Z_{line,1}} - 1)I_{G0}$	V_{GC}
Line-to-line (A-B)	$I_{GA} - I_{GB}$	$V_{GA} - V_{GB}$
Line-to-line (B-C)	$I_{GB} - I_{GC}$	$V_{GB} - V_{GC}$
Line-to-line (C-A)	$I_{GC} - I_{GA}$	$V_{GC} - V_{GA}$

If the source impedance Z_G and Z_H are not known in advanced, they can be estimated using Equations 2.16 and 2.17.

$$Z_G = -\frac{V_G - V_{G,prefault}}{I_G - I_{G,prefault}} \tag{2.16}$$

$$Z_H = -\frac{V_H - V_{H,prefault}}{I_H - I_{H,prefault}} \tag{2.17}$$

For unbalanced faults such as single line-to-ground and line-to-line faults, I_G and V_G are defined as in Table 2.1 [7]. The subscript A, B, C, 1, and 0 stand for phase A, phase B, phase C, positive-sequence, and zero-sequence quantities, respectively.

2.2 Two-ended Impedance-based Methods

Two-ended impedance-based methods estimate the fault location using the measurements taken at both ends of the line. The basic idea is to write Kirchhoff's voltage law from both ends of the line [6]. The location estimate

is given as Equation 2.18.

$$m = \frac{V_G - V_H + Z_{line,1} I_H}{(I_G + I_H) Z_{line,1}} \tag{2.18}$$

If the measurements are not synchronized, the fault location can be estimated by using the magnitude of the measurements. The location estimate is given by Equation 2.19 [2].

$$m = \frac{-B \pm \sqrt{B^2 - 4AC}}{2A} \tag{2.19}$$

where,

$$a + jb = V_G \tag{2.20}$$

$$c + jd = Z_{line} I_G \tag{2.21}$$

$$e + jf = V_H - Z_{line} I_H \tag{2.22}$$

$$g + jh = Z_{line} I_H \tag{2.23}$$

$$A = c^2 + d^2 - g^2 - h^2 \tag{2.24}$$

$$B = -2 \times (ac + bd + eg + fh) \tag{2.25}$$

$$C = a^2 + b^2 - e^2 - f^2 \tag{2.26}$$

The value of m that lies between 0 and 1 pu is chosen to be the location estimate.

For unbalanced faults, it is possible to use the negative-sequence quantities for Equations 2.18 and 2.19. This method is referred to as the two-terminal(two-ended) negative-sequence method.

Chapter 3

Removing Exponential Decaying DC Offset in Current Waveforms

The fault locating methods introduced in Chapter 2 are calculated using the voltage and current phasors. However, the voltage and current measurements are recorded in time-series and must be converted to phasors before applying the fault locating methods. This Chapter discusses the effect of exponential decaying DC offset present at current waveforms which prevents accurate phasor calculations. An approach to remove the DC offset is proposed to accurately calculate the phasor of the measurements.

3.1 Phasor Conversion Using Fourier Transform

The Fourier transform transforms time domain signals into frequency domain using sinusoids as its basis function. The Fourier transform of input signal is given by Equation 3.1.

$$X(\Omega) = \int_{-\infty}^{\infty} x(t) e^{-j\Omega t} dt \tag{3.1}$$

The Fourier transform represents time-sequence data as linear combinations of sinusoidal functions. The function is the frequency response of

the input signal which can be further separated into magnitude spectrum ($|X(\Omega)|$) and phase spectrum ($\angle|X(\Omega)|$). The magnitude spectrum measures the amount and the phase spectrum measures the location of the input signal with comparison to the sinusoidal basis functions. A sinusoidal signal can be converted into phasor form using the magnitude spectrum and phase spectrum of Fourier analysis.

The Fourier transform is efficient when analyzing stationary signals, where the statistical parameters such as mean and variance do not change over time. For power disturbance signals, 1 cycle (50 or 60 Hz) input data points are usually sufficient for phasor conversion given they are stationary.

3.2 DC Offset in Transient Fault Signals

Consider an RL circuit such as the one shown in Figure 3.1. The circuit represents a three-phase short circuit fault. The current during the fault is calculated and is shown in Equation 3.2.

$$i(t) = \sqrt{2} \times \frac{V_{rms}}{\sqrt{R^2 + X^2}} \left[\sin(wt + \beta - \theta) - \sin(\beta - \theta) e^{\frac{-\omega t}{X/R}}\right] \tag{3.2}$$

where β is the fault incidence angle and θ is the system impedance angle.

The equation shows that the fault current can be decomposed into a symmetrical AC component and an exponentially decaying DC component as in Equations 3.3 and 3.4. The asymmetrical component will be referred to as the DC offset throughout the Chapter. Equation 3.4 implies that the DC offset will have maximum impact on the total fault current when fault incidence angle

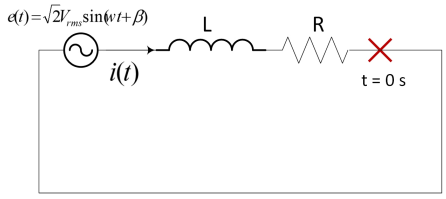

Figure 3.1: Fault Current in Series RL Circuit.

and the system impedance angle differ by 90°, that is $\beta = \theta + 90°$. Note that the harmonics may be present in the symmetrical AC component. However, they are not written in Equation 3.3 for simplicity.

$$i_{ac} = \sqrt{2} \times \frac{V_{rms}}{\sqrt{R^2 + X^2}} [\sin(wt + \beta - \theta)] \tag{3.3}$$

$$i_{dc} = \sqrt{2} \times \frac{V_{rms}}{\sqrt{R^2 + X^2}} \left[-\sin(\beta - \theta) e^{\frac{-\omega t}{X/R}} \right] \tag{3.4}$$

3.3 Proposed Approach to Remove DC Offset from Transient Fault Signals

The frequency response at 60 Hz (or 50 Hz) should be applied at the symmetrical portion of the fault signals for accurate phasor calculations. However, the fault data measurements can only be available for a short period of time. For example, only 2∼3 cycles might be available for temporary faults. The DC offset is likely to be present within the given amount of measurements.

As discussed previously, the fault current can be decomposed into an AC component and a DC component as shown in Equation 3.5.

$$i = i_{ac} + i_{dc} \tag{3.5}$$

For simplicity, the DC component is re-written as in Equation 3.6

$$i_{dc} = Ae^{wt/\tau} \tag{3.6}$$

where $A = -\frac{V_{rms}}{\sqrt{R^2+X^2}}\left[-sin(\beta-\theta)\right]$ and $\tau = X/R$. The two parameters A and τ will be referred to as the peak DC offset magnitude and the X/R ratio.

The following procedures are presented to remove the DC offset from a signal. The main idea is to remove the DC offset in time-domain by estimating two parameters A and τ and reconstruct i_{dc}. Then the reconstructed i_{dc} can be removed from the original signal so that Fourier transform can be applied to the symmetrical component of the fault signals.

1. Select Two Pairs of Data Points

   First pick two pairs of data points from the fault signal. The first pair is arbitrarily selected with a margin of Δ. The second pair is separated from the first pair by the sampling frequency N. An example is shown in Figure 3.2

2. Estimate X/R Ratio

   After four data points are selected, The estimated X/R ratio is derived by the following procedure and given in Equation 3.11.

$$i[t_{Ref}] - i[t_{Ref+N}] = Ae^{w[t_{Ref}]/\tau} - Ae^{w[t_{Ref+N}]/\tau} \tag{3.7}$$

$$i[t_{Ref+\Delta}] - i[t_{Ref+N+\Delta}] = Ae^{w[t_{Ref+\Delta}]/\tau} - Ae^{w[t_{Ref+N+\Delta}]/\tau} \tag{3.8}$$

$$\frac{i[t_{Ref}] - i[t_{Ref+N}]}{i[t_{Ref+\Delta}] - i[t_{Ref+N+\Delta}]} = \frac{Ae^{w[tRef]/\tau} - Ae^{w[t_{Ref+N}]/\tau}}{Ae^{w[t_{Ref+\Delta}]/\tau} - Ae^{w[t_{Ref+N+\Delta}]/\tau}} \tag{3.9}$$

$$= e^{-wt_{\Delta}/\tau} \tag{3.10}$$

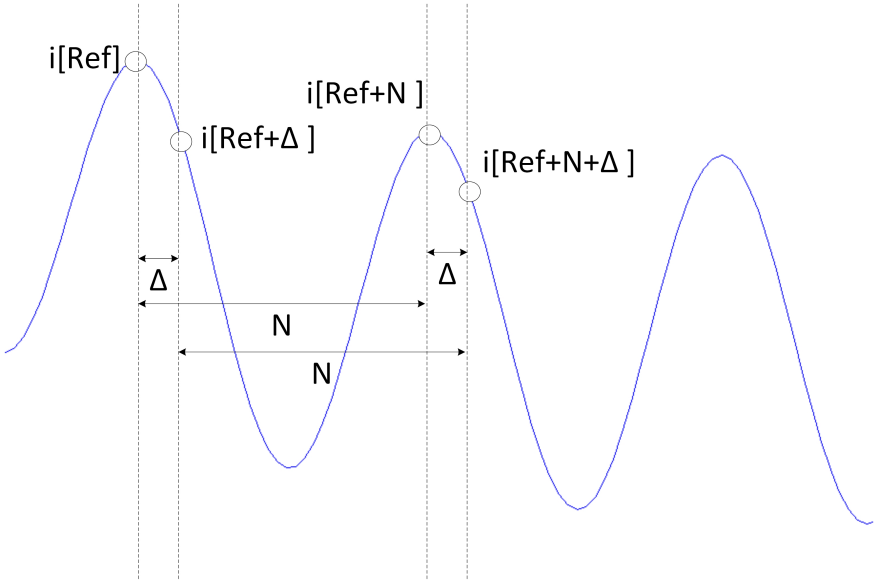

Figure 3.2: Four data points for DC Offset Removal.

$$\tau_{est} = -\frac{wt_{\Delta}}{ln\frac{i[t_{Ref}]-i[t_{Ref+N}]}{i[t_{Ref+\Delta}]-i[t_{Ref+N+\Delta}]}} \tag{3.11}$$

Note that even if the harmonics were present in the fault signals, they will be canceled out by subtracting the current values separated by the sampling frequency N. This is an advantage over other methods [8,9] that assumes the number of harmonics in the fault signal before removing the DC offset.

3. Estimate the Peak DC Offset Magnitude

   Next, estimate the peak DC offset magnitude using the estimated X/R ratio. This is done by substituting τ_{est} into τ defined in Equation 3.8

$$A_{est} = \frac{i[t_{Ref+\Delta}] - i[t_{Ref+N+\Delta}]}{e^{w[t_{Ref+\Delta}]/\tau_{est}} - e^{w[t_{Ref+N+\Delta}]/\tau_{est}}} \tag{3.12}$$

4. Remove the DC Offset from the Measurements

   Since τ and A are estimated from Equations 3.11 and 3.12 the DC offset can be reconstructed using Equation 3.13.

$$i_{dc,est} = A_{est} e^{wt/\tau_{est}} \tag{3.13}$$

   The symmetrical AC component of the current is then derived from Equation 3.14.

$$i_{ac,est} = i - i_{dc,est} \tag{3.14}$$

The proposed approach can accurately remove DC offset given that the fault signals are clean and the signal can be decomposed into AC and DC components perfectly. However for noisy signals, the X/R ratio and the peak DC offset magnitude estimated from Equation 3.11 and Equation 3.8 may be variable. Therefore, the following procedure gives a more robust estimation of the X/R ratio and the peak DC offset magnitude for noisy measurements.

1. Vary the size of the Δ in Equation 3.11 and estimate X/R ratios for multiple values of Δ.

2. Select the median value of all the possible X/R ratios calculated. Use the median value as the estimated X/R ratio. Remove outliers beforehand if necessary.

3. Use the estimated X/R ratio and estimate possible peak DC offset magnitudes using multiple values of Δ and Equation 3.12. Take the median value as the estimated peak DC offset magnitude.

4. Reconstruct the DC offset and remove the DC offset from the Measurements.

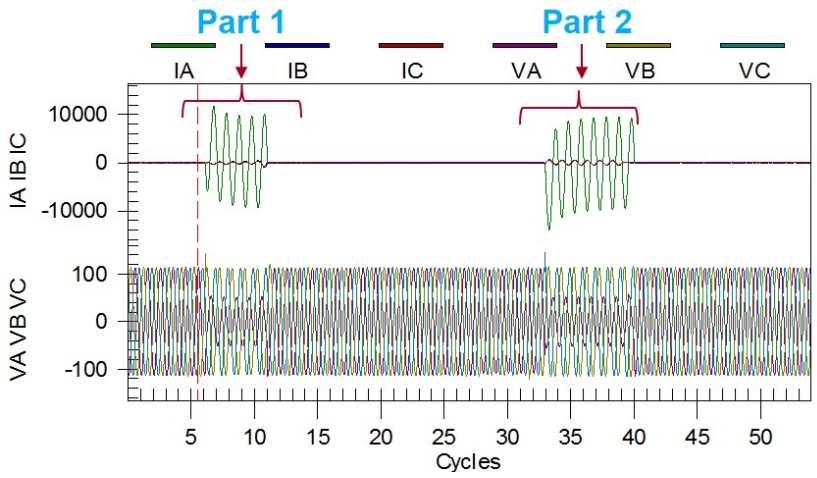

Figure 3.3: Event 1: A-G Fault, 1/1/13, 09:38:33.94.

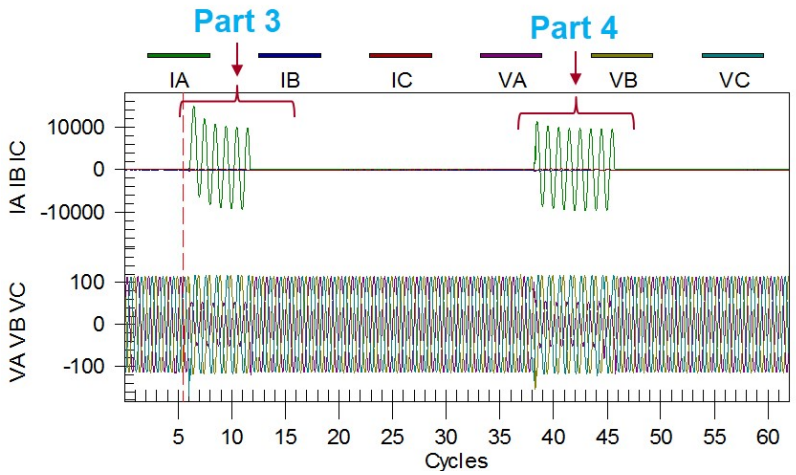

Figure 3.4: Event 2: A-G Fault, 1/1/13, 09:42:23.08.

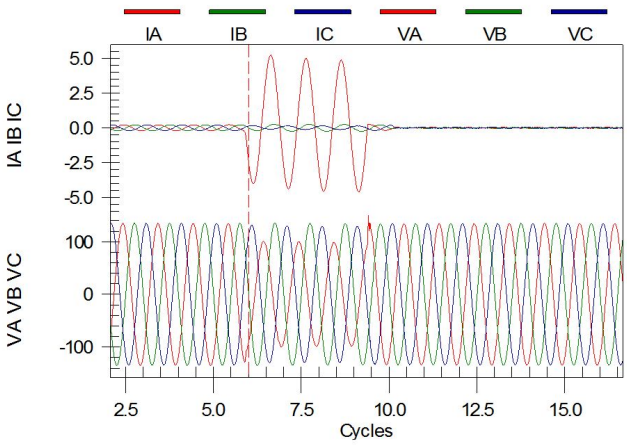

Figure 3.5: Event 3: A-G Fault, 4/27/12, 00:48:11 .

3.4 Application of Proposed Method to Actual Circuit Data

The approach proposed in the previous sections is applied to three fault event data files. The first two event files are part of a permanent fault where two recloser operations are recorded in each event file. The recloser ultimately locks out after four operations. Voltage and current waveforms of the events are shown in Figure 3.3 and Figure 3.4. The third event file is a lightning event and is shown in Figure 3.5. The description proposed in the previous section is applied to these event files.

1. The peak point of the first lobe after the fault incidence is chosen to be the reference point, i[Ref]. Every integer value between 10 and 50 is selected as Δ. The data points used for estimating the model parameters are illustrated in Figure 3.6.

2. Using the sets of four data points, the possible X/R ratios are calculated. The histograms of the possible X/R ratios are depicted in Figure 3.7. The median value is selected as the estimated X/R ratio. Note that for event 3, the negative X/R ratios are considered as outliers and are excluded before applying the median.

3. Similarly, the histogram of the possible peak DC offset magnitude is plotted in Figure 3.8. Again, the median of these values is used as the estimated peak DC offset magnitude.

4. DC offset is reproduced using the estimated X/R ratio and the estimated peak DC offset magnitude. Figure 3.9 show the waveforms after the DC offsets are removed.

5. Figure 3.10 shows the magnitude response of the measurements before (red lines) and after (blue lines) the DC offset removal. Then, fault location is estimated by the Takagi method and is shown in Figure 3.11. The blue lines show more robust and less fluctuating magnitude response and location estimates than the red lines.

Table 3.1: Estimated Parameters.

Estimated Parameter	Event 1 (Part 1)	Event 1 (Part 2)	Event 3 (Part 3)	Event 2 (Part 4)	Event 3
X/R Ratio	5.906634	5.646981	6.471046	5.664295	10.46782
Peak DC Offset Mag.	-4.477568	5.463019	-7.050961	-2.165794	-1.89091

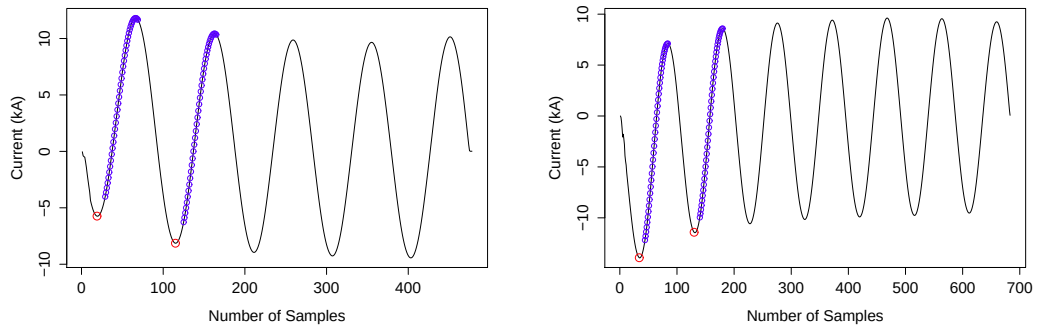

(a)

(b)

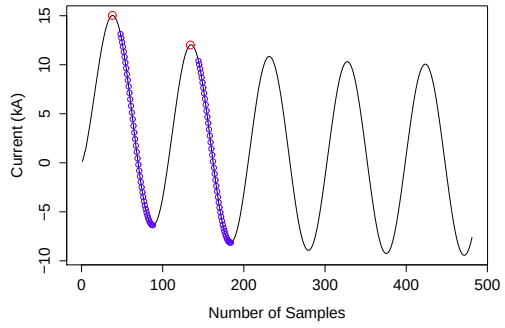

(c)

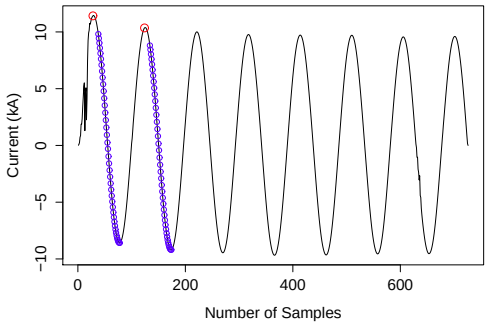

(d)

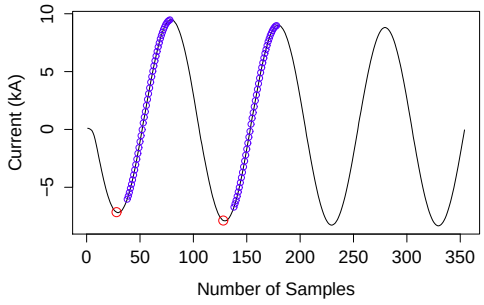

(e)

Figure 3.6: Selected Data Points for (a) Event 1 (Part 1), (b) Event 1 (Part 2), (c) Event 2 (Part 3), (d) Event 2 (Part 4), and (e) Event 3.

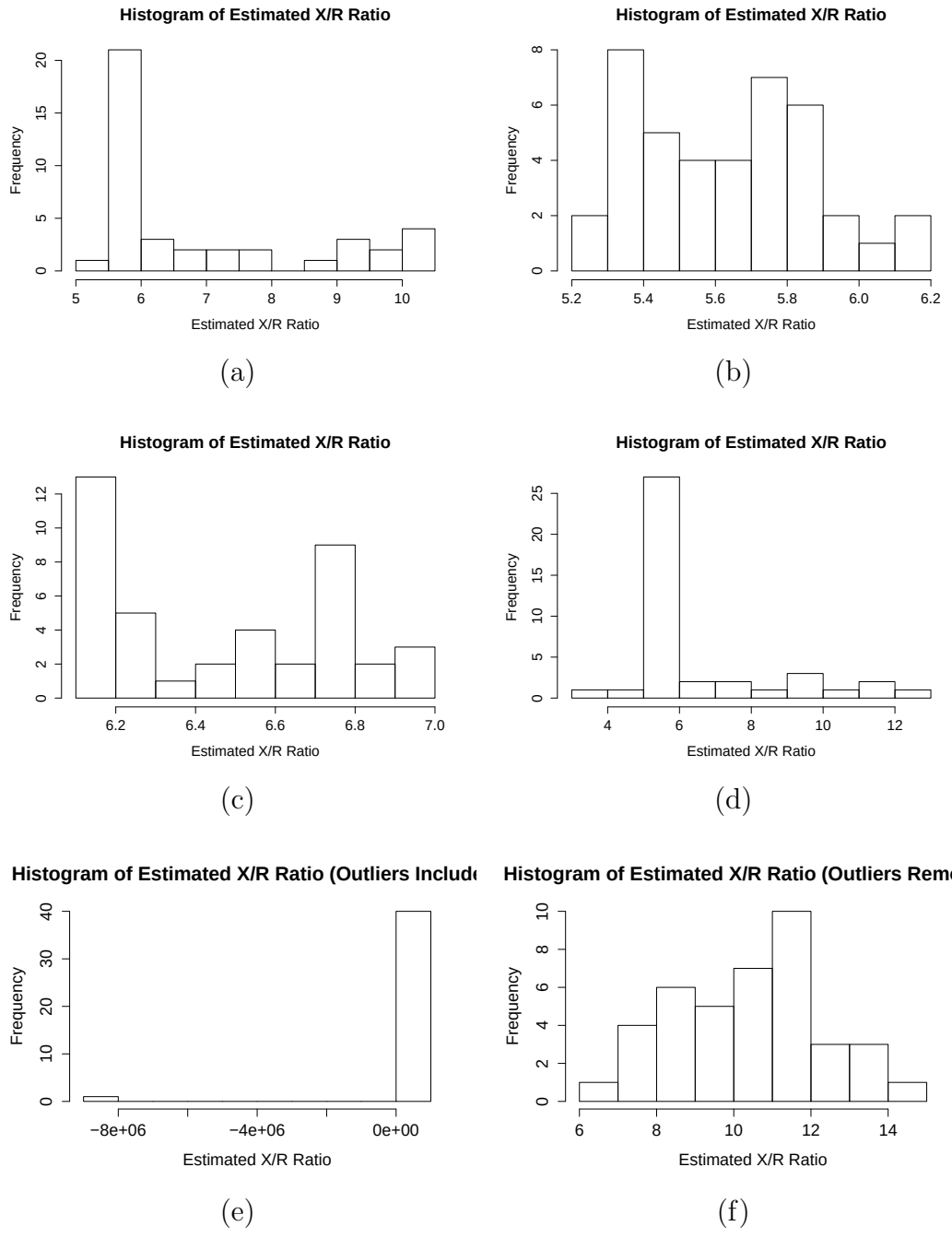

Figure 3.7: Histogram of Estimated X/R Ratios for (a) Event 1 (Part 1), (b) Event 1 (Part 2), (c) Event 2 (Part 3), (d) Event 2 (Part 4), and (e) Event 3.

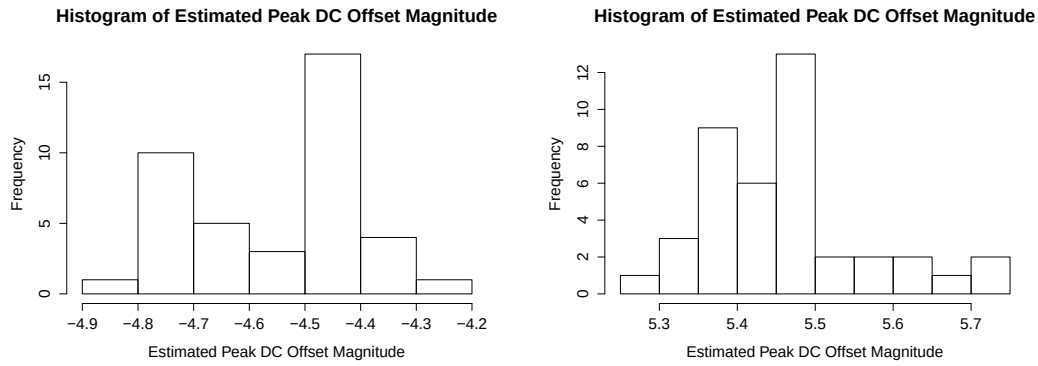

(a)

(b)

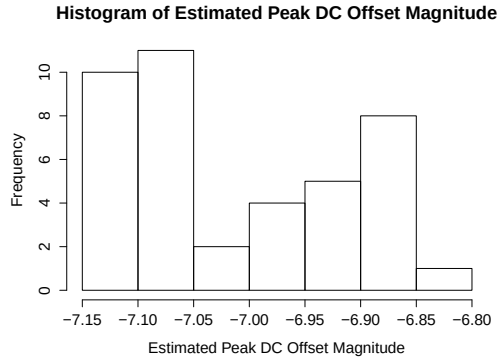

(c)

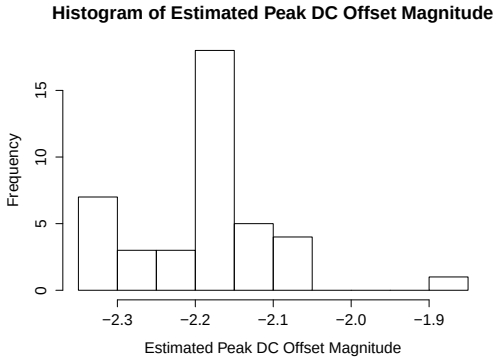

(d)

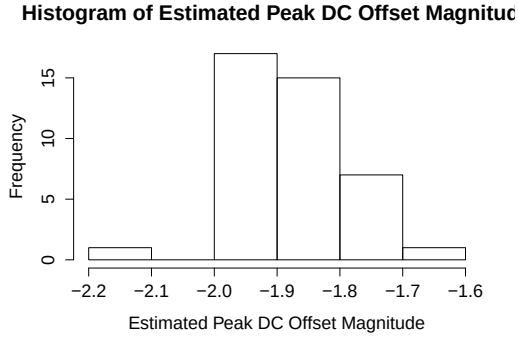

(e)

Figure 3.8: Histogram of Estimated Peak DC Offset Magnitude for (a) Event 1 (Part 1), (b) Event 1 (Part 2), (c) Event 2 (Part 3), (d) Event 2 (Part 4), and (e) Event 3.

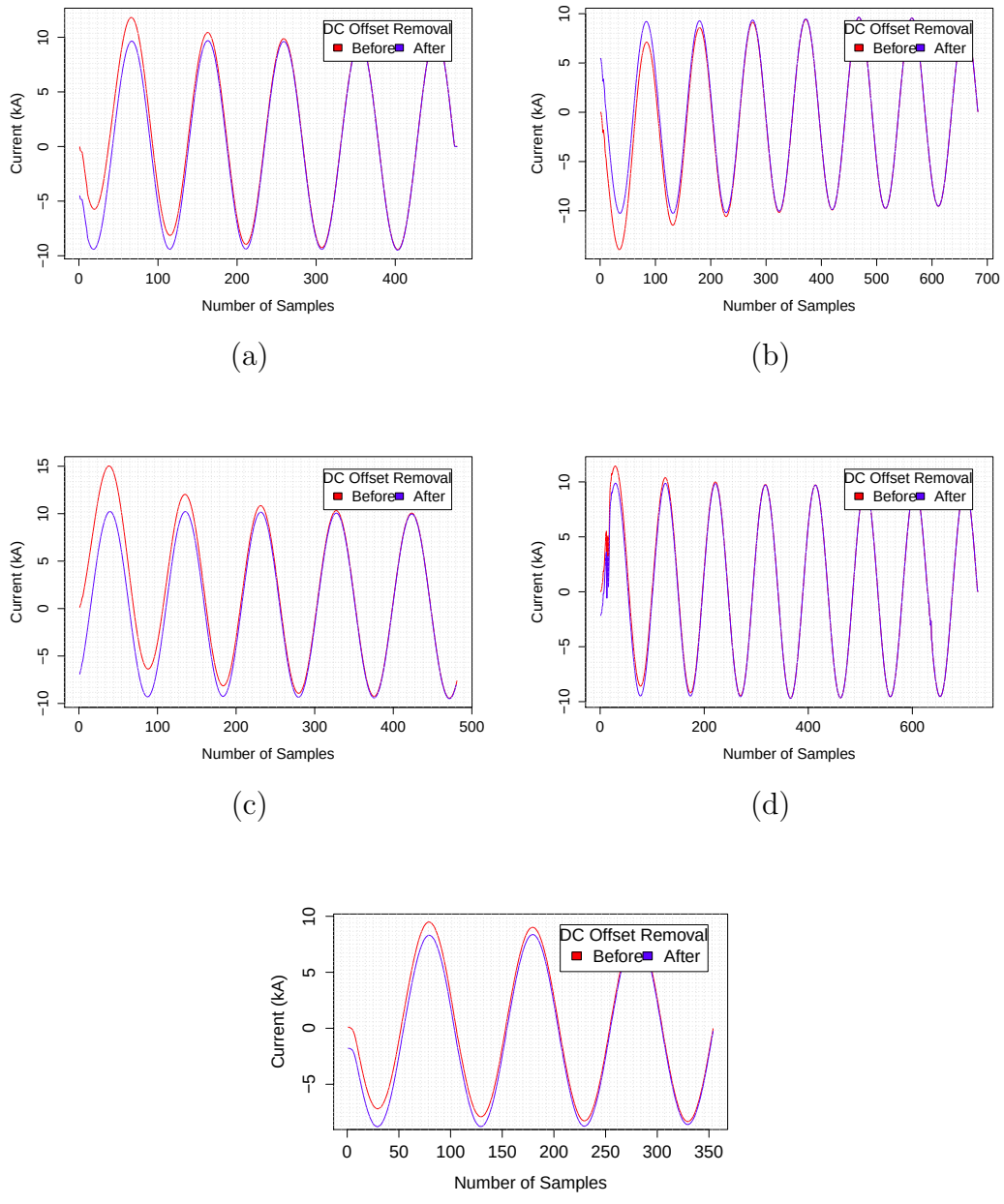

Figure 3.9: DC Offset Removal: (a) Event 1 (Part 1), (b) Event 1 (Part 2), (c) Event 2 (Part 3), (d) Event 2 (Part 4), and (e) Event 3.

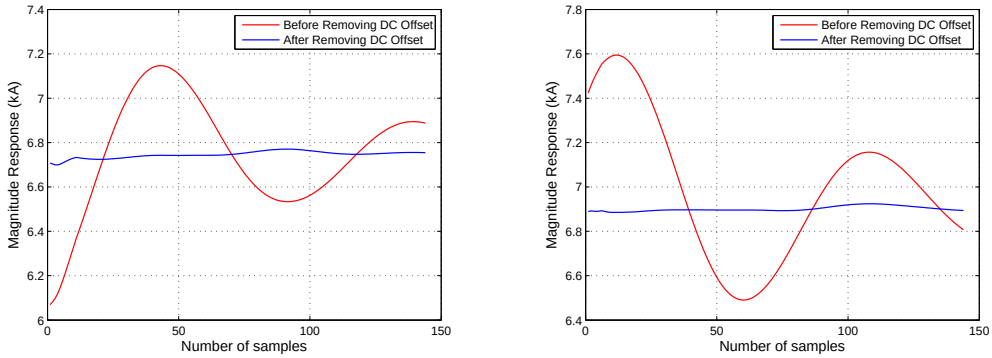

(a)

(b)

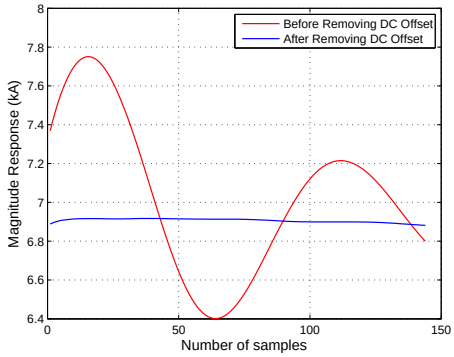

(c)

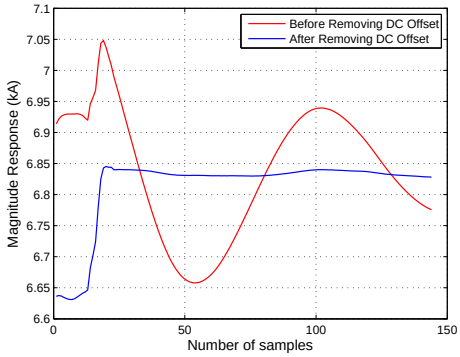

(d)

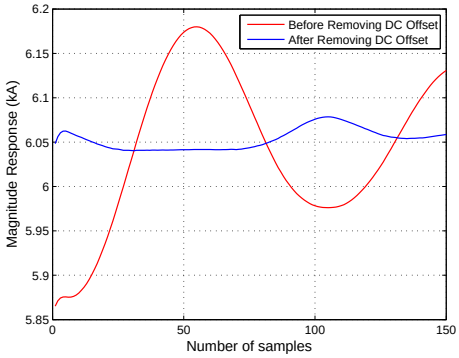

(e)

Figure 3.10: Magnitude Response Before and After Removing DC Offset: (a) Event 1 (Part 1), (b) Event 1 (Part 2), (c) Event 2 (Part 3), (d) Event 2 (Part 4), and (e) Event 3.

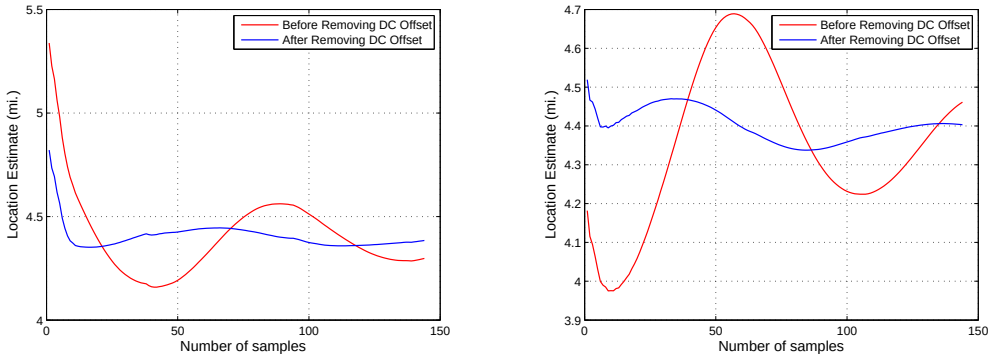

(a)

(b)

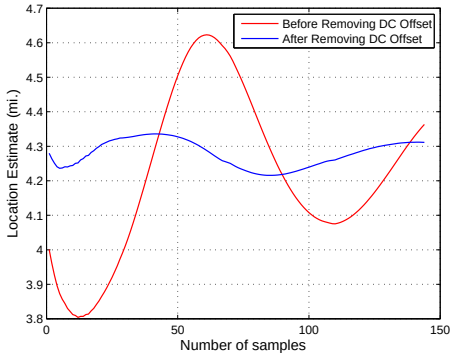

(c)

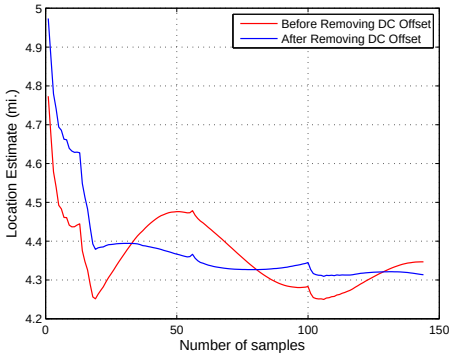

(d)

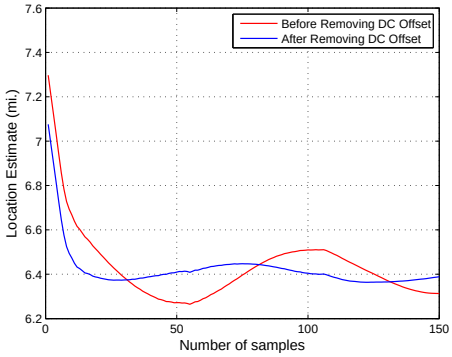

(e)

Figure 3.11: Fault Location Estimated by Takagi Method Before and After Removing DC Offset: (a) Event 1 (Part 1), (b) Event 1 (Part 2), (c) Event 2 (Part 3), (d) Event 2 (Part 4), and (e) Event 3.

Chapter 4

Improved Method for Locating Faults Upstream from Distributed Generation

Fault locating in distribution systems with distributed generation (DG) is discussed in this Chapter. One-ended impedance-based methods are normally used in distribution systems assuming that the line is radial. However, when a DG is connected to the distribution line, the generator will contribute fault currents and thus affects the apparent impedance calculated from the local substation. Since the penetration of DG is expected to increase, fault locating in distribution systems with DG needs to be examined.

Fault locating in the system can be considered in two scenarios: Fault located upstream from DG and fault located downstream from DG. Many improved algorithms have been proposed for locating faults that are downstream from DG [10–12]. However, they consider less on the impact of DG when a fault is located upstream from DG. This Chapter focuses on improving the fault location estimates when faults are located upstream from DG.

4.1 Fault Locating Approach in Distribution Systems with Distributed Generation

Consider a distribution system shown in Figure 4.1. The substation and a local synchronous generator are connected at the point of interconnection (POI). The load is represented as a single lumped load at the remote end. The measurements are assumed to be available from the substation and the DG terminals.

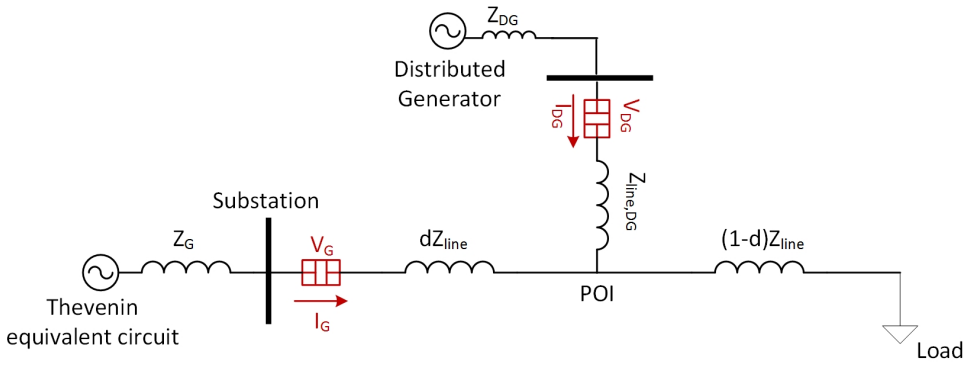

Figure 4.1: One-line diagram of a distribution system with distributed generation.

4.1.1 Estimated Voltage at POI as a Reference

The estimated voltage at the POI can be used as a reference point in determining whether a fault has occurred upstream or downstream from DG. Suppose a fault occurred. Then estimate the voltage at the POI by calculating the voltage drop from the substation and DG measurements to the POI, independently. If the estimated voltage values at the POI are the same,

the fault is considered to be downstream from DG. If the estimated voltage values at the POI are not the same, the fault is considered to be upstream from DG.

If the measurements at the substation and DG are not synchronized, the POI can also serve to be a reference point to synchronize the measurements [5] [7] . Using the pre-fault measurements from the substation and DG, the synchronization operator $e^{j\theta}$ can be derived as in Equation 4.2.

$$V_G - I_G \times dZ_{line} = V_{DG}e^{j\theta} - I_{DG}e^{j\theta} \times Z_{line,DG} \tag{4.1}$$

$$e^{j\theta} = \frac{V_G - I_G \times dZ_{line}}{V_{DG} - I_{DG} \times Z_{line,DG}} \tag{4.2}$$

It should be noted that in an actual system tapped loads along the distribution feeder do introduce error in determining the relative location of the fault or in calculating the synchronization operator. The following sections assume that the measurements from the substation and the DG have been synchronized.

4.1.2 Locating Faults Upstream from DG

When the fault is located upstream from DG, the DG at the remote end of the line contributes a fault current in addition to the fault current flowing from the substation. The fault current contribution from the DG will shift the angle between I_f and I_G in Equation 2.2.

Therefore the remote current infeed from the DG will increase the reactance error in the simple reactance and the Takagi methods. The Eriksson

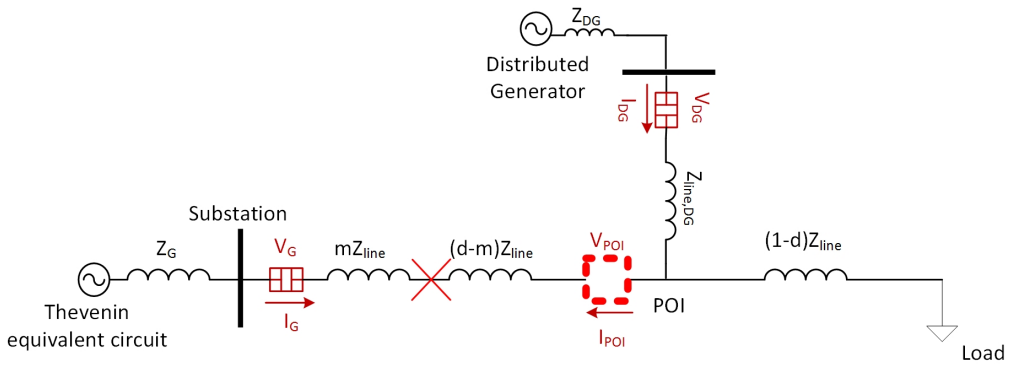

Figure 4.2: Fault is located upstream from DG.

method and the two-ended method will not be effected by the fault current contribution because they take into account the fault current contribution from the remote end.

However, the two-ended method requires remote end measurements. The Eriksson method also requires the remote end measurement in order to estimate the remote source impedance, if not known in advance. Therefore it would be beneficial to have the remote end measurements to apply these methods. One solution is to use the measurements at the DG terminal as the remote end measurements. However if this measurements are used, the current flowing from the POI to the load is neglected.

An improved method is described as follows. A virtual monitor is assumed to be present in the POI facing the substation as shown in Figure 4.2. Then pre-fault (subscripted *pre*) and during-fault measurements (subscripted *flt*) captured at this monitor can be estimated using the measurements taken at the substation and the DG.

The pre-fault and during-fault voltage measurements are estimated using the healthy line section connecting the DG and the POI.

$$V_{pre,POI} = V_{pre,DG} - I_{pre,DG} \times Z_{line,DG} \tag{4.3}$$

$$V_{flt,POI} = V_{flt,DG} - I_{flt,DG} \times Z_{line,DG} \tag{4.4}$$

The pre-fault current measurement is estimated as the opposite direction of the pre-fault current measured at the substation side. The during-fault current measurement is estimated by subtracting the load current from the fault current flowing from the DG. Assuming a constant impedance load Z_{load}, the load impedance can be estimated as in Equation 4.7.

$$I_{pre,POI} = -I_{pre,G} \tag{4.5}$$

$$I_{flt,POI} = I_{flt,DG} - \frac{V_{flt,POI}}{(1-d)Z_{line} + Z_{load}} \tag{4.6}$$

$$Z_{load} = \frac{V_{pre,G} - I_{pre,G} \times dZ_{line}}{I_{pre,G} + I_{pre,DG}} - (1-d)Z_{line} \tag{4.7}$$

The measurements from this virtual monitor can be used in the application of the two-ended method and can provide the remote source impedance for the Eriksson method. The remote source impedance is estimated as Equation 4.8 and this value can be used as the Z_H value in Equations 2.8, 2.9, 2.10.

$$Z_{s,remote} = -\frac{V_{flt,POI} - V_{pre,POI}}{I_{flt,POI} - I_{pre,POI}} \tag{4.8}$$

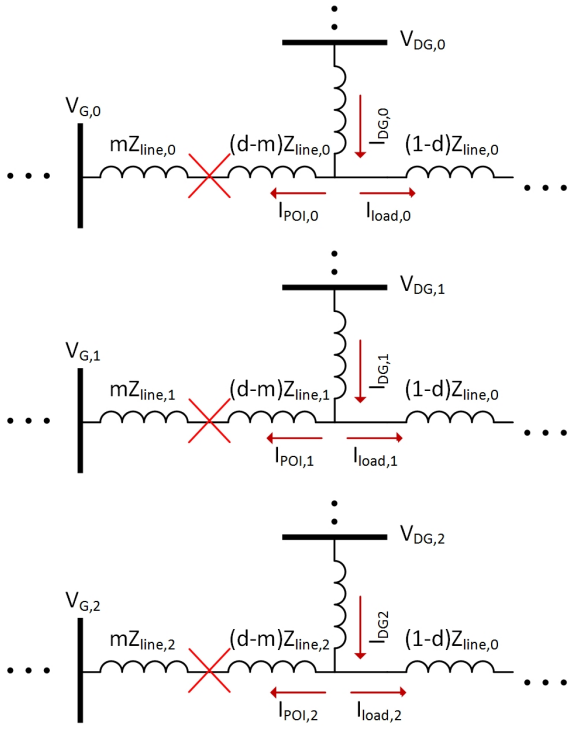

Figure 4.3: Symmetrical components calculations.

Note that Equations 4.3 - 4.8 are written in case where the faults are balanced. For unbalanced faults, the equations should be applied for every positive-sequence, negative-sequence, and zero-sequence components as shown in Figure 4.3.

4.2 Application of Proposed Fault Locating Approach on Simulated Fault Data

A PSCAD/EMTDC model is developed to test the fault locating methods in a distribution system with a distributed generation. The nominal volt-

Table 4.1: Simulation Model Parameters

Model Parameter	Value
$Z_{G,1}$	$j3.8088\ \Omega$
$Z_{G,0}$	$j11.4264\ \Omega$
$Z_{DG,1}$	$j1.28547\ \Omega$
$Z_{DG,0}$	$j0.5967\ \Omega$
$Z_{line,1}$	$0.2780 + j0.6584\ \Omega$/mile
$Z_{line,0}$	$0.5474 + j1.9720\ \Omega$/mile
$Z_{line,DG,1}$	$0.2780 + j0.6584\ \Omega$/mile
$Z_{line,DG,0}$	$0.5474 + j1.9720\ \Omega$/mile
Substation transformer	138/13.8 kV, 10 MVA, 4%
DG transformer	6.9/13.8 kV, 8 MVA, 4%
Sampling Frequency	128 samples per cycle

age of the feeder is 13.8 kV and the distribution feeder is 6 miles long. A synchronous distributed generator is interconnected to the middle of the feeder which is 3 miles away from the substation. Two different load consumption scenarios are considered. The first scenario assumes that the loads are lumped at the remote end consuming 10.62 MVA at 0.9 power factor lagging. This modeling resembles an express feeder where the loads are concentrated at some distances from the substation [13]. In the second scenario, the loads are distributed along the distribution feeder. The loads are connected at 1.5, 3, 4.5, and 6 miles from the substation and the loads consume 3.54, 3.31, 3.14, 3.07 MVA, all at 0.9 power factor lagging, respectively. For each scenario, single line-to-ground faults with two different fault resistance values, 1 and 5 ohms, are simulated. The system parameters are modeled using [14] and are summa-

rized in Table 4.1. The subscript *1* and *0* are referred to as positive-sequence and zero-sequence values.

The location estimate and the percent error are summarized in Table 4.2 and Table 4.3. The percent error is calculated using Equation 4.9. The simple reactance method and the Takagi method are applied using measurements from the substation. The Eriksson method and the two-ended method are applied in two different manners: one using the substation and the DG measurements and the other using the substation and the estimated POI measurements as explained in Section 4.1.2. The two-ended method is applied using negative-sequence components (see Chapter 2) to estimate the fault location.

$$\text{Error } \% = \frac{\text{Estimated Location - Actual Location}}{\text{Total Length of the Feeder}} \times 100 \qquad (4.9)$$

As described in the previous sections, the simple reactance method is the least accurate among the fault locating methods. It is effected by the load and the remote infeed when fault resistance is present. On the other hand, the Takagi method improves the estimate accuracy by taking into account the load currents into the location estimate. However, when DG is located downstream from the fault, the remote infeed from the DG will effect the fault location estimated by the Takagi method.

Therefore the focus is on applying the Eriksson method and the negative-sequence method since these methods take into account both the load current and the remote infeed. However, when these methods are applied using the substation and the DG measurements, they give considerable error. The er-

rors come from the inaccuracy of the remote source impedance for the Eriksson method, and the load currents drawn by the loads at the remote end for the two-ended method. It is found in Table 4.2(b) that if the Eriksson method is applied using the substation and the DG measurements, it gives 3.83% and 7.50% error for each simulated fault distance. The two-ended method using the substation and the DG measurements shows consistent location estimates with respect to fault resistance, but the estimates have an offset of 1.17% and 1.00% due to the load currents drawn from the remote end. By using the estimated measurements at the POI in place of the DG measurements, the errors in the Eriksson method and the two-ended method are reduced to at most 0.33 % for all simulation cases.

Table 4.3 summarizes the fault location estimates when the load is distributed along the distribution feeder. Again, the Eriksson method and the two-ended method using the substation and the POI measurements show the most robust and accurate estimates. In this scenario, the source of error comes from the loads placed between the substation and the POI.

Table 4.2: Fault location estimated from the substation for the lumped load scenario (a) $R_f = 1$ (b) $R_f = 5$

(a)

$R_f = 1$	Actual Location (1 mi.)		Actual Location (2 mi.)	
	Estimate (mi.)	Error (%)	Estimate (mi.)	Error (%)
Simple reactance	0.93	-1.17	1.91	-1.50
Takagi	1.03	0.50	2.04	0.67
Eriksson (Substation + DG)	1.04	0.67	2.08	1.33
Neg.-sequence (Substation + DG)	0.93	-1.17	1.94	-1.00
Eriksson (Substation + POI)	1.00	0.00	2.00	0.00
Neg.-sequence (Substation + POI)	1.00	0.00	2.00	0.00

(b)

$R_f = 5$	Actual Location (1 mi.)		Actual Location (2 mi.)	
	Estimate (mi.)	Error (%)	Estimate (mi.)	Error (%)
Simple reactance	1.00	0.00	2.03	0.50
Takagi	1.15	2.50	2.19	3.17
Eriksson (Substation + DG)	1.23	3.83	2.45	7.50
Neg.-sequence (Substation + DG)	0.93	-1.17	1.94	-1.00
Eriksson (Substation + POI)	0.98	-0.33	2.00	0.00
Neg.-sequence (Substation + POI)	1.00	0.00	2.00	0.00

Table 4.3: Fault location estimated from the substation for the distributed loads scenario (a) $R_f = 1$ (b) $R_f = 5$

(a)

$R_f = 1$	Actual Location (1 mi.)		Actual Location (2 mi.)	
	Estimate (mi.)	Error (%)	Estimate (mi.)	Error (%)
Simple reactance	0.94	-1.00	1.93	-1.17
Takagi	1.05	0.83	2.06	1.00
Eriksson (Substation + DG)	1.06	1.00	2.10	1.67
Neg.-sequence (Substation + DG)	0.94	-1.00	1.96	-0.67
Eriksson (Substation + POI)	1.01	0.17	2.02	0.33
Neg.-sequence (Substation + POI)	1.01	0.17	2.02	0.33

(b)

$R_f = 5$	Actual Location (1 mi.)		Actual Location (2 mi.)	
	Estimate (mi.)	Error (%)	Estimate (mi.)	Error (%)
Simple reactance	1.04	0.67	2.06	1.00
Takagi	1.22	3.67	2.26	4.33
Eriksson (Substation + DG)	1.30	5.00	2.52	8.67
Neg.-sequence (Substation + DG)	0.94	-1.00	1.96	-0.67
Eriksson (Substation + POI)	1.05	0.83	2.08	1.33
Neg.-sequence (Substation + POI)	1.01	0.17	2.02	0.33

Chapter 5

Application of Fault Locating Methods in Utility Circuit

Fault locating methods presented in Chapter 2 are applied to distribution circuits with distributed generation operating in interconnected grid and microgrid modes. A time-domain model which represents the distribution circuit is developed based on system parameters provided by participating utilities. The circuit consists of the 34.5-kV AT - WF No. 207 Line, OV and WF 4.8-kV circuits, and the two local generating facilities, 416-kW Box Farm and 6.6-MW WN wind farm. The circuit is designed to be operated in microgrid depending on the location of where a permanent fault occur. Oneline diagrams of the utility circuit operating in interconnected mode and microgrid mode are illustrated in Figures 5.1, 5.2, and 5.3. This chapter presents the application of fault locating methods in interconnected grid and microgrid operation using data obtained from the time-domain model.

5.1 Application of Fault Locating Methods in Interconnected Operation

This section evaluates the accuracy and robustness of fault locating methods in interconnected grid operation using the time-domain model. The

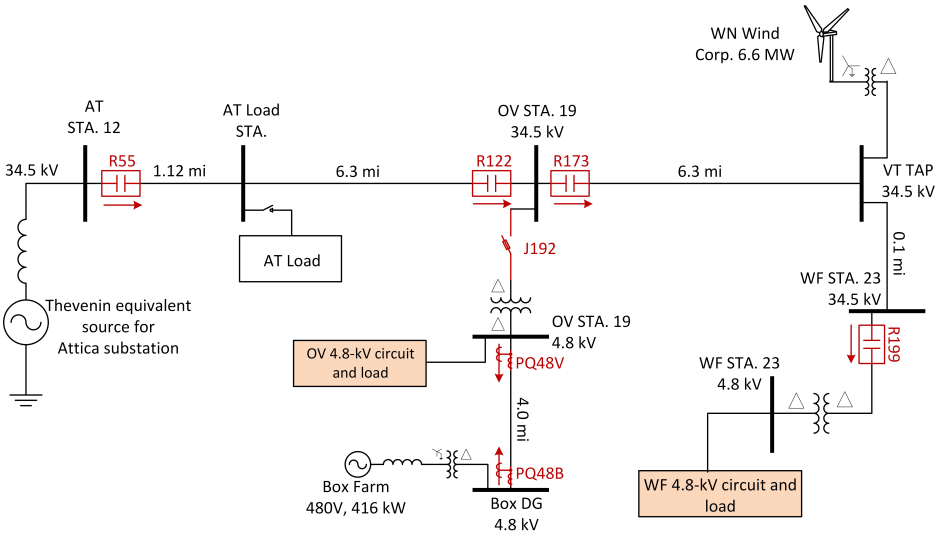

Figure 5.1: Utility Circuit Operating in Interconnected Mode.

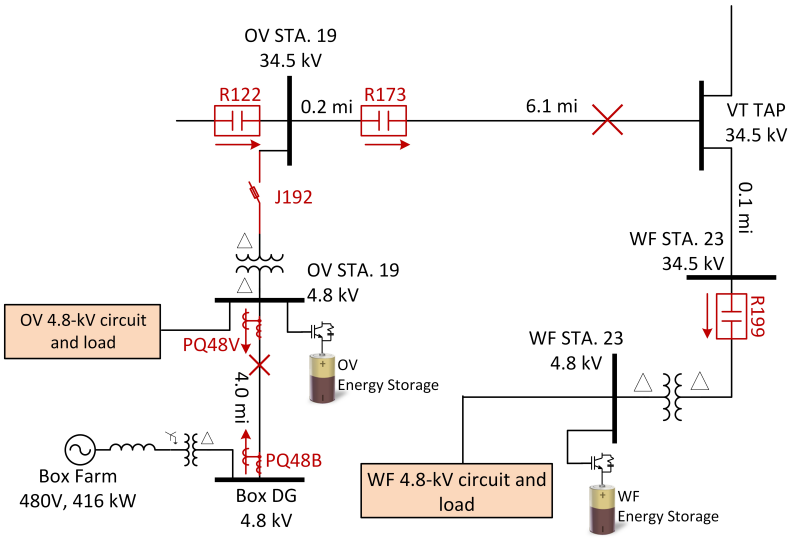

Figure 5.2: Utility Circuit Operating in OV-WF Microgrid.

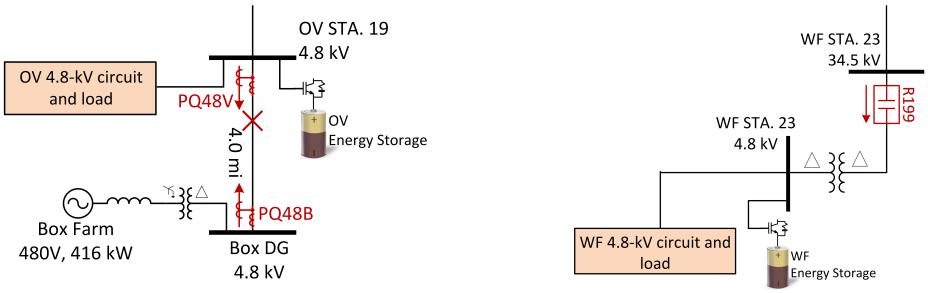

(a) OV Microgrid (b) WF Microgrid

Figure 5.3: Utility Circuit operating in (a) OV Microgrid and (b) WF Microgird

one-line diagram of the model is shown in Figure 5.4. Three short-circuit fault scenarios (Scenarios G1, G2, and G3) are considered for different segments of the distribution line.

1. Scenario G1 : Multiple single line-to-ground faults with fault resistances of 0 and 5 ohms are simulated in Line Section 1 between R55 and R122. These faults are located 0.5, 1.12, 2.38, and 5.32 miles from recloser R55.

2. Scenario G2: Multiple single line-to-ground faults with resistance of 0 and 5 ohms are simulated in Line Section 2 downstream from R173. These faults are located 1.9, 4.84, and 6.10 miles from recloser R173.

3. Scenario G3: Multiple line-to-line faults with resistance of 0 and 5 ohms are simulated in Line Section 3 between PQ48V and PQ48B. These faults are located 0.8 and 2.67 miles from PQ48V.

Line-to-line faults are simulated in Scenario G3 because single line-to-ground faults between PQ48V and PQ48B would not result in any fault

current as the 4.8-kV line is ungrounded. Voltage and current waveforms during fault conditions are captured by digital relays in each recloser (R55, R122, R173, and R199) and by the two power quality monitors (PQ48B and PQ48V). Waveforms of one or more faulted phases are then used in fault locating methods implemented in MATLAB. Table 5.1 lists methods used in estimating fault locations for Scenarios G1, G2, and G3.

Table 5.1: Fault Locating Methods Applied for Evaluation Scenarios.

Scenario	Applied Method	
G1	One-ended method	Simple Reactance Method Takagi Method Novosel et al. Method
	Two-ended Method	Negative-sequence Method (Unynchronized)
G2	One-ended Method	Simple Reactance Method Takagi Method Novosel et al. Method
G3	One-ended method	Simple Reactance Method Takagi Method Eriksson Method
	Two-ended Method	Negative-sequence Method (Unynchronized)

5.1.1 Line Impedance

Fault locating methods introduced in Chapter 2 assume uniform line impedance for the entire line in which the fault current flows. Unfortunately the line impedance of Line Section 1 and Line Section 2 is non-uniform because

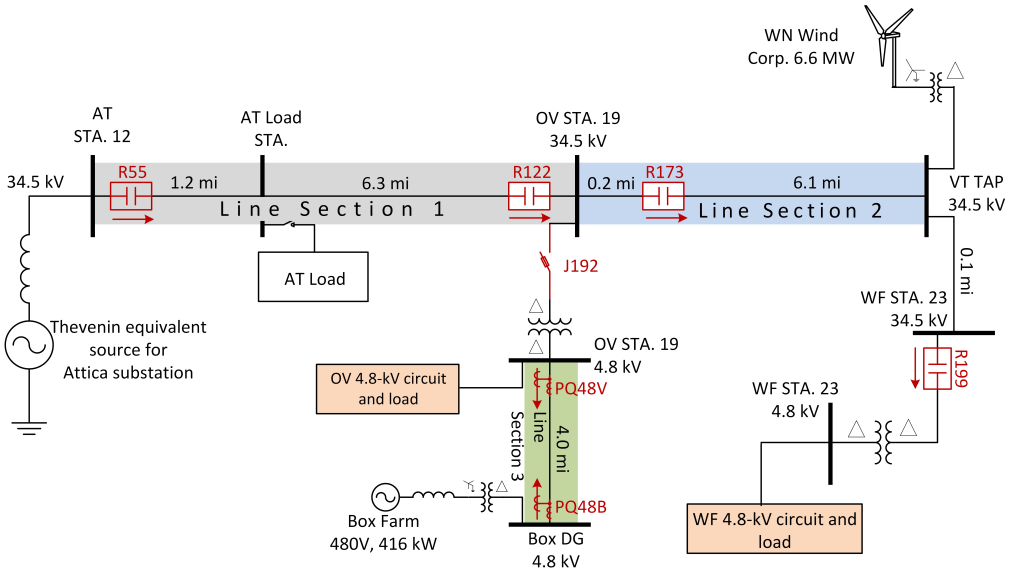

Figure 5.4: One-line Diagram Showing Line Sections for Evaluating Scenarios G1, G2, and G3.

each is made up of two different line configurations. To apply fault locating methods, each section is assumed to be uniform with the line impedance per mile of the longer segment representing the entire section. It should be noted that this assumption does introduce error to the location estimate. The line impedances of the Line Sections 1, 2, and 3 for applying fault locating methods are specified in Table 5.2.

5.1.2 Input Data and Steady-State Condition

The time-domain model is used to simulate short-circuit faults in Scenarios G1, G2, and G3. Each simulation run starts from time zero and reaches its normal operating condition prior to applying a fault condition. Steady-state

load demand and the power output of the two distributed generators are shown in Table 5.3 and Table 5.4, respectively.

Table 5.2: Impedances of the 207 Line.

	From Bus	To Bus	Line Length (mi)	Line Impedance (ohms/mi)	Assumption (ohms/mi)
Line Section 1 (G1)	AT Sta.12 34.5 kV	AT Load 34.5 kV	1.12	P : 0.4379 + j0.6621 Z : 0.7216 + j3.1595	P : 0.8001 + j0.8119 Z : 1.0600 + j2.9353
	AT Load 34.5 kV	OV 34.5 kV	6.3	P : 0.8001 + j0.8119 Z : 1.0600 + j2.9353	
Line Section 2 (G2)	OV 34.5 kV	Recloser R173	0.2	P : 0.8826 + j0.8676 Z : 1.1562 + j3.1030	P : 0.8826 + j0.8676 Z : 1.1562 + j3.1030
	Recloser R173	VT TAP 34.5 kV	6.1	P: 0.8826 + j0.8676 Z : 1.1562 + j3.1030	
	VT TAP 34.5 kV	WF 34.5 kV	0.1	P : 0.977 + j0.9610 Z : 1.280 + j3.4340	
Line Section 3 (G3)	OV 4.8 kV	Box DG 4.8 kV	4.0	P : 0.9927 + j1.1478 Z : 0.9927 + j1.1478	P : 0.9927 + j1.1478 Z : 0.9927 + j1.1478

Note: P and Z are positive- and zero-sequence impedances, respectively.

Table 5.3: Pre-fault Load Demand.

AT Substation		AT Load		OV		WF	
P (MW)	Q (Mvar)	P (MW)	Q (Mvar)	P (MW)	Q (Mvar)	P (MW)	Q (Mvar)
4.5635	2.2067	2.0359	1.2992	1.3985	0.5611	1.7274	0.9659

Table 5.4: Pre-fault DG Outputs.

Box Farm		WN Wind Farm	
P (MW)	Q (Mvar)	P (MW)	Q (Mvar)
0.4159	-0.1277	6.7261	-2.6247

A fault condition is then applied at 1.6 s following the start of the simulation (t_f = 1.6 s). A typical fault current waveform captured by the upstream recloser protecting the line section is illustrated in Figure 5.5. It

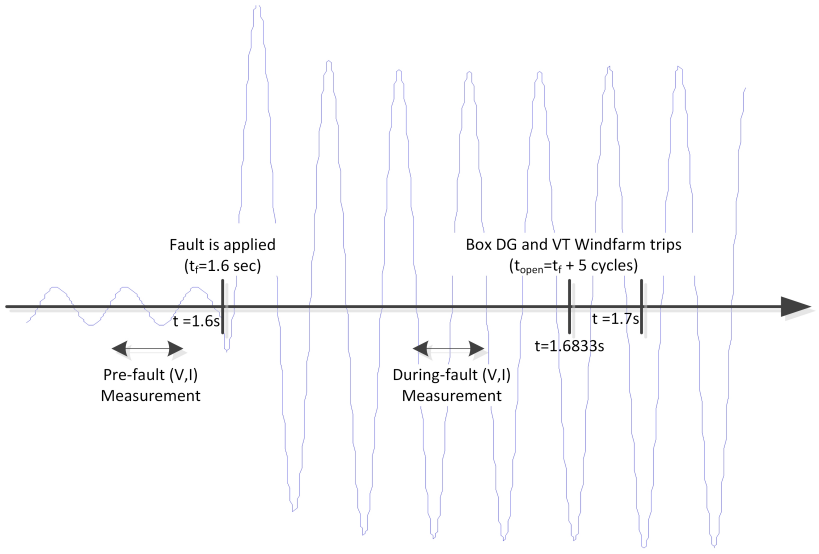

Figure 5.5: One-line Diagram Showing Line Sections for Evaluating Scenarios G1, G2, and G3.

shows pre-fault and during-fault portions of the entire waveform. Immediately following the fault condition, both Box Farm and WN wind farm contribute fault currents. In the simulation, it is assumed that both generators will trip open at 5 cycles, i.e., $t_{tripped} = t_f + 5$ cycles. At this time instant, the upstream recloser may or may not open yet. This study assumes waveforms between t_f and $t_{tripped}$ are captured by real world digital relays and power quality monitoring devices. Pre-processing procedures are then performed to determine faulted phases and the portion of waveforms to use for fault locating. Due to the DC offset in the fault current, the during-fault measurements used in the fault locating methods are taken approximately three cycles after the fault is applied. Figure 5.5 shows a fault current waveform beyond $t_{tripped}$,

however, only the waveform portion between t_f - 2 cycles and t_f + 5 cycles is used for fault locating.

Table 5.5 shows reclosers and power quality monitors providing fault event data for each evaluation scenario. The two-ended negative-sequence method is applied for Scenario G1 and G3. They use fault event data captured by the reclosers upstream and downstream from the fault.

Table 5.5: Measurement Locations.

Scenario	Simple Reactance	Takagi	Novosel	Eriksson	Negative-sequence
G1	R55	R55	R55	N/A	R55 and R122
G2	R173 or R122	R173 or R122	R173 or R122	N/A	N/A
G3	PQ48V or PQ48B	PQ48V or PQ48B	N/A	PQ48V or PQ48B	PQ48V and PQ48B

5.1.3 Evaluation of Fault Locating Methods for Scenario G1

A single line-to-ground fault is applied at four different locations on Line Section 1 with a fault resistance of 0 and 5 ohms. These locations are 0.5, 1.12, 2.38, and 5.32 miles from recloser R55. The pre-fault current flowing through Line Section 1 is about 86 A and the fault current recorded by R55 is about 1 kA to 2 kA depending on the location of the fault. Fault event waveforms captured by R55 and R122 are then used to estimate the fault location using various fault locating methods. Results of location estimates

along with their errors are shown in Table 5.6. The example current and voltage waveforms for Scenario G1 are shown in Figure 5.6.

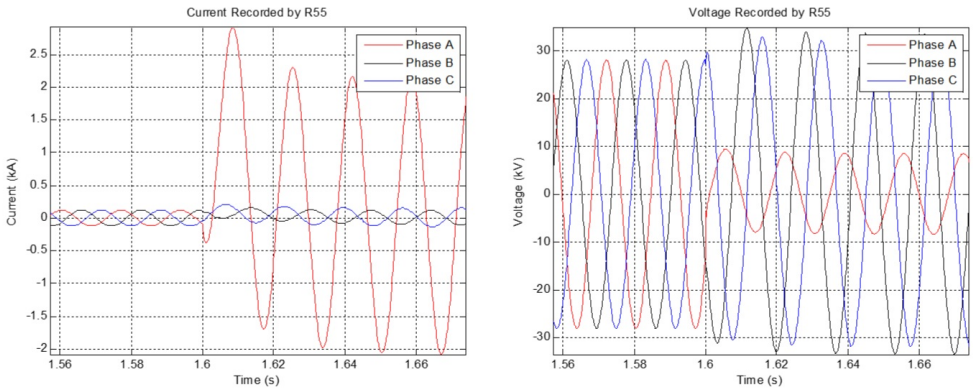

Figure 5.6: Current and Voltage Waveforms Recorded by R55 for Scenario G1.

The simple reactance method is the simplest to implement and as seen in Table 5.6, it also is the least accurate. It requires only voltage and current measurements from one end, in this case R55. It estimates the fault location by taking the ratio of imaginary portion of apparent impedance to the imaginary portion of line impedance. However, since the method assumes that I_f and I_G are in-phase (see Chapter 2), any fault resistance can greatly affect the accuracy of the estimates. Table 5.6 indicates that error increases to more than 10% when fault resistance of 5 ohms is applied. Percent error is calculated using Equation 5.1.

$$\text{Error } \% = \frac{\text{Estimated Location - Actual Location}}{\text{Total Length of the Feeder}} \times 100 \qquad (5.1)$$

The Takagi method improves the accuracy of the simple reactance method by using the pre-fault current values to account for load currents.

Table 5.6: Application of Fault Locating Methods in Scenario G1

(a)

	Actual Location (0.50 mi.)		Actual Location (1.12 mi.)	
	$R_f = 0\ \Omega$ Estimate (%Error)	$R_f = 5\ \Omega$ Estimate (%Error)	$R_f = 0\ \Omega$ Estimate (%Error)	$R_f = 5\ \Omega$ Estimate (%Error)
Simple Reactance	0.52 (0.27)	-0.35 (-11.46)	1.17 (0.67)	0.32 (-10.78)
Takagi	0.49 (-0.13)	0.51 (0.13)	1.10 (-0.27)	1.13 (0.13)
Novosel	0.49 (-0.13)	0.58 (1.08)	1.10 (-0.27)	1.20 (1.08)
Negative-sequence	0.41 (-1.21)	0.39 (-1.48)	0.87 (-3.37)	0.85 (-3.64)

(b)

	Actual Location (2.38 mi.)		Actual Location (5.32 mi.)	
	$R_f = 0\ \Omega$ Estimate (%Error)	$R_f = 5\ \Omega$ Estimate (%Error)	$R_f = 0\ \Omega$ Estimate (%Error)	$R_f = 5\ \Omega$ Estimate (%Error)
Simple Reactance	2.46 (1.08)	1.59 (-10.65)	5.42 (1.35)	4.54 (-10.51)
Takagi	2.38 (0.00)	2.38 (0.00)	5.33 (0.13)	5.27 (-0.67)
Novosel	2.37 (-0.13)	2.47 (1.21)	5.32 (0.00)	5.40 (1.08)
Negative-sequence	2.14 (-3.23)	2.13 (-3.37)	5.11 (-2.83)	5.11 (-2.83)

Therefore the Takagi method will produce an error if there are fault contributions from the Box Farm and the WN wind farm. For this method, the error is small because the remote end does not contribute fault current (delta-delta connected transformers block the zero-sequence fault current contribution from the Box Farm and the WN wind farm). The results show that the Takagi method can be accurate and provides a vast improvement over the simple reactance method. The Novosel et al. method utilizes pre-fault voltage and current values to estimate the load impedance and the source impedance. Using the estimates, the Novosel et al. method provides accurate estimation

irrespective of fault resistance, load currents, and source impedances. The results in Table 5.6 show that the Novosel et al. method is accurate to within a 1.5%. The two-ended negative-sequence method is also implemented. Using this method, the fault location estimate was accurate to within 3.64%. The error comes from the non-homogeneity of the line section.

The percentage differences between the actual fault location and the estimate as calculated by Equation 5.1 are depicted in Figure 5.7. The simple reactance method stands out as giving the worst location estimate with an error of 10 to 12 percent. The other methods perform equally resulting in an estimate deviating from the actual fault location by no more than 4 percent.

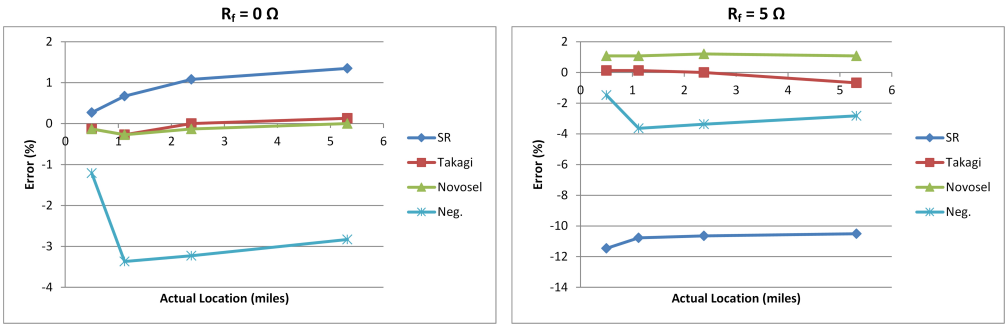

Figure 5.7: Errors in Location Estimates for Scenario G1.

5.1.4 Evaluation of Fault Locating Methods for Scenario G2

A single line-to-ground fault, with fault resistance of 0 and 5 ohms, is applied at three different locations on Line Section 2. The pre-fault current flowing through Line Section 2 is about 100 A and the fault current recorded

Table 5.7: Application of Fault Locating Methods in Scenario G2 Using (a) R173 and (b) R122

(a)

	Actual Location (1.90 mi.)		Actual Location (4.84 mi.)		Actual Location (6.10 mi.)	
	$R_f = 0\,\Omega$ Estimate (%Error)	$R_f = 5\,\Omega$ Estimate (%Error)	$R_f = 0\,\Omega$ Estimate (%Error)	$R_f = 5\,\Omega$ Estimate (%Error)	$R_f = 0\,\Omega$ Estimate (%Error)	$R_f = 5\,\Omega$ Estimate (%Error)
Simple Reactance	1.90 (0.00)	0.98 (-14.84)	4.83 (-0.16)	3.90 (-15.16)	6.09 (-0.16)	5.15 (-15.32)
Takagi	1.90 (0.00)	1.65 (-4.03)	4.83 (-0.16)	4.48 (-5.81)	6.09 (-0.16)	5.70 (-6.45)
Novosel	1.90 (0.00)	1.94 (0.65)	4.83 (-0.16)	4.86 (0.32)	6.08 (-0.32)	6.11 (0.16)

(b)

	Actual Location (1.90 mi.)		Actual Location (4.84 mi.)		Actual Location (6.10 mi.)	
	$R_f = 0\,\Omega$ Estimate (%Error)	$R_f = 5\,\Omega$ Estimate (%Error)	$R_f = 0\,\Omega$ Estimate (%Error)	$R_f = 5\,\Omega$ Estimate (%Error)	$R_f = 0\,\Omega$ Estimate (%Error)	$R_f = 5\,\Omega$ Estimate (%Error)
Simple Reactance	2.08 (-0.31)	1.11 (-15.47)	4.96 (-1.25)	3.97 (-16.72)	6.20 (-1.56)	5.18 (-17.50)
Takagi	2.08 (-0.31)	1.85 (-3.91)	4.98 (-0.94)	4.65 (-6.09)	6.21 (-1.41)	5.83 (-7.34)
Novosel	2.09 (-0.16)	2.11 (0.16)	4.99 (-0.78)	4.98 (-0.94)	6.22 (-1.25)	6.20 (-1.56)

by R173 is about 500 A to 750 A depending on the location of the fault. Since the fault is downstream of both R173 and R122, one-ended methods are implemented using data from each recloser. The results are tabulated in Table 5.7. The current and voltage waveforms are similar to those shown in Figure 5.6.

For bolted faults, the differences between the methods were negligible. When there is resistance to the fault, the Novosel et al. method provided the most accurate estimate of the fault location while the simple reactance and the Takagi methods had high percent error. Using data from R173 should provide

a more accurate estimate of the fault location than with data from R122, because it is unaffected by infeed from Box Farm. However, the simulation indicates that the difference is minimal for single line-to-ground faults because the fault current contribution from Box Farm is blocked by the delta-delta connected transformer.

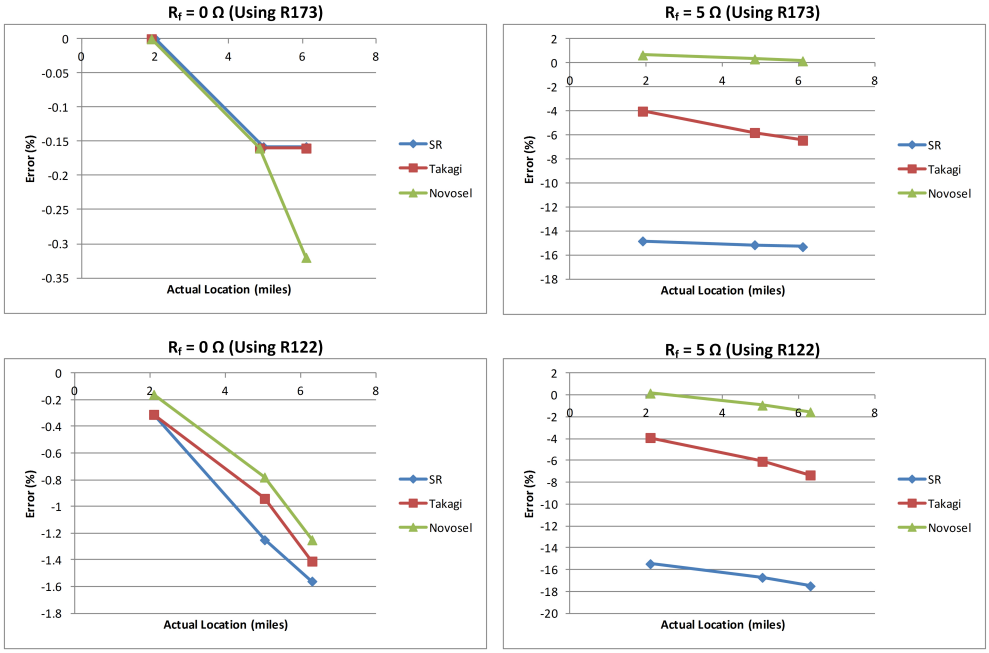

Figure 5.8: Errors in Location Estimates for Scenario G2 Using Data Captured at R173 and R122.

5.1.5 Evaluation of Fault Locating Methods for Scenario G3

A line-to-line fault is simulated at two locations of Line Section 3 with fault resistance of 0 ohms and 5 ohms. The pre-fault current flowing through Line Section 3 is about 50 A and the fault current recorded by PQ48B is about

150 A to 350 A depending on the location of the fault. Since both ends of the line contribute fault current, the two-ended method methods are applicable using data from PQ48B and PQ48V. The one-ended methods are implemented using the data from PQ48B with the exception of the Eriksson method. This is because the Eriksson method may provide two feasible location estimates between 0 and 1 per-unit distance (see Chapter 2) using data from PQ48B when fault resistance is high. For these scenarios, the Eriksson method using data from PQ48V is used to determine the correct estimate. The results for the one-ended methods recorded in Table 5.8 reflect results using PQ48V. The example current and voltage waveforms for Scenario G3 are shown in Figure 5.9.

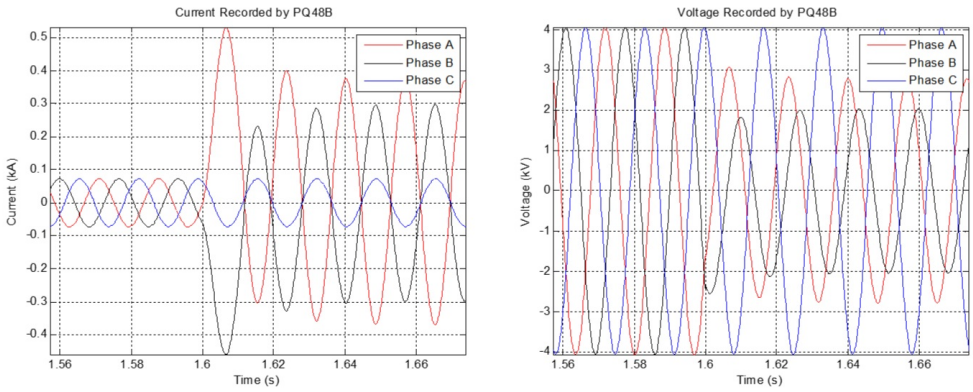

Figure 5.9: Current and Voltage Waveforms Recorded by PQ48B for Scenario G3.

Both the simple reactance and the Takagi methods result in large errors in their estimates for faults with non-zero resistance. It should be noted that the Takagi method is less accurate than the simple reactance method. In order

Table 5.8: Application of Fault Locating Methods in Scenario G3

	Actual Location (0.80 mi.)		Actual Location (2.67 mi.)	
	$R_f = 0\ \Omega$ Estimate (%Error)	$R_f = 5\ \Omega$ Estimate (%Error)	$R_f = 0\ \Omega$ Estimate (%Error)	$R_f = 5\ \Omega$ Estimate (%Error)
Simple Reactance	0.80 (0.00)	1.38 (14.5)	2.67 (0.00)	2.41 (-6.5)
Takagi	0.80 (0.00)	2.06 (31.5)	2.67 (0.00)	4.31 (41)
Eriksson	0.80 (0.00)	0.80 (0.00)	2.67 (0.00)	2.67 (0.00)
Negative-sequence	0.80 (0.00)	0.80 (0.00)	2.67 (0.00)	2.67 (0.00)

to account for the effect of the system load, the Takagi method subtracts the pre-fault load current from the fault current. However, when the fault is applied in Line Section 3, the actual load current drawn by the system differs from the pre-fault current that the Takagi method subtracts, adding considerably to the error. As a result, the Takagi method fails to give an accurate location estimate. On the other hand, the Eriksson method and the two-ended negative-sequence method are robust to fault resistance, load, and remote infeed and provide accurate results.

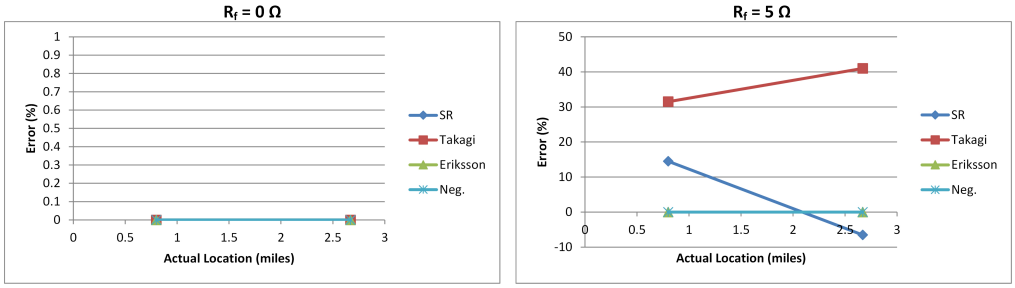

Figure 5.10: Errors in Location Estimates for Scenario G3.

5.2 Application of Fault Locating Methods in Microgrid Operation

This section evaluates the accuracy and robustness of fault locating methods in microgrid operation using the time-domain model. The one-line diagram of Microgrid OW is shown in Figure 5.11. Microgrid OW can be further separated into two distinct microgrids (Microgrid O and Microgrid W). Fault locating methods are applied to three scenarios: two for faults in the Microgrid OW (Scenarios OW1 and OW2) and one for a fault in the Microgrid O (Scenario O1). Fault locating is not considered for Microgrid W, however, it can be developed in a similar fashion if desired.

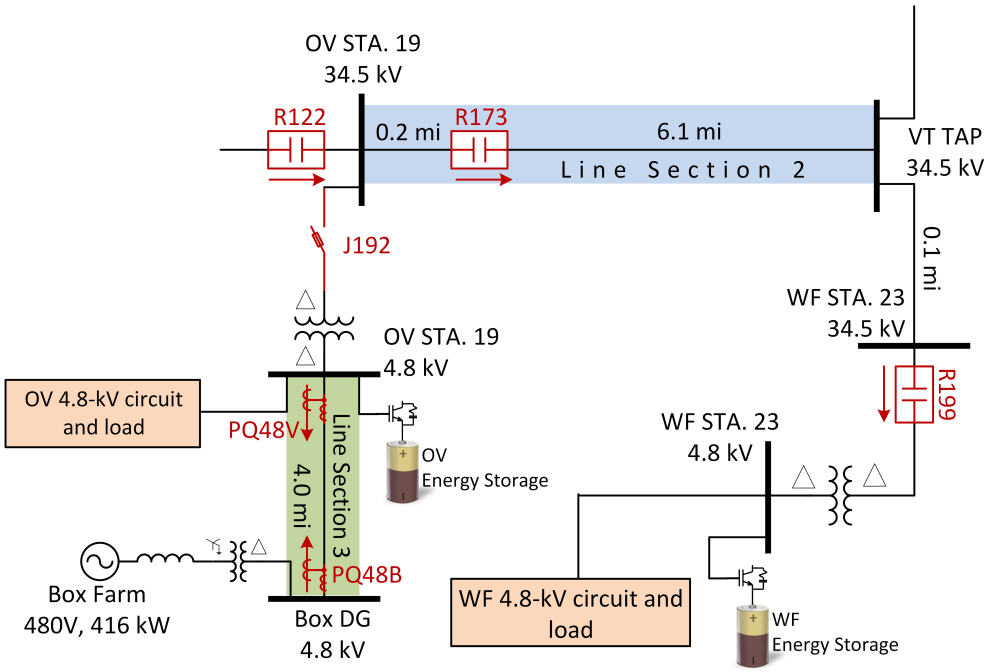

Figure 5.11: One-line diagram of Microgrid OW.

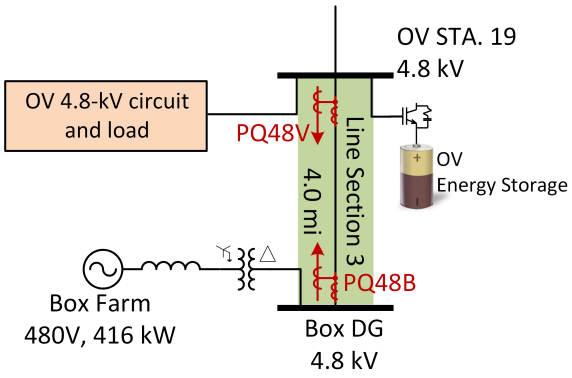

Figure 5.12: One-line diagram of Microgrid O.

1. Scenario OW1: Multiple line-to-line faults with fault resistances of 0 and 5 ohms are simulated in Line Section 2 when operating in Microgrid OW. Theses faults are located 1.9, 4.84, and 6.10 miles from recloser R173.

2. Scenario OW2: Multiple line-to-line faults with fault resistance of 0 and 5 ohms are simulated in Line Section 3 when operating in Microgrid OW. These faults are located 0.8 and 2.67 miles from PQ48B.

3. Scenario O1: Multiple line-to-line faults with fault resistance of 0 and 5 ohms are simulated in Line Section 3 when operating in Microgrid O. These faults are located 0.8 and 2.67 miles from PQ48B.

It should be noted that single line-to-ground faults would not result in any fault currents since the transformers in Line Sections 2 and 3 are delta connected. Voltage and current values are captured by digital relays in each recloser (R173 and R199) and by the two power quality monitors (PQ48B and

PQ48V). The fault location methods implemented are listed in Table 5.9.

Table 5.9: Fault Locating Methods Applied for Evaluation Scenarios.

Scenario	Applied Method	
OW1	One-ended method	Simple Reactance Method Takagi Method Novosel et al. Method
OW2	One-ended method	Simple Reactance Method Takagi Method Novosel et al. Method
O1	One-ended method	Simple Reactance Method Takagi Method Novosel et al. Method

5.2.1 Line Impedance

Line Section 2 consists of two different line configurations and thus the line impedance is non-homogenous. Therefore, as described in Section 5.1.1, the line impedance per mile of the longer line is used over the entire line section. The line data is specified in Table 5.10.

Table 5.10: Impedances of the 207 Line.

	From Bus	To Bus	Line Length (mi)	Line Impedance (ohms/mi)	Assumption (ohms/mi)
Line Section 2 (OW1)	OV 34.5 kV	Recloser R173	0.2	P : 0.8826 + j0.8676 Z : 1.1562 + j3.1030	P : 0.8826 + j0.8676 Z : 1.1562 + j3.1030
	Recloser R173	VT TAP 34.5 kV	6.1	P: 0.8826 + j0.8676 Z : 1.1562 + j3.1030	
	VT TAP 34.5 kV	WF 34.5 kV	0.1	P : 0.977 + j0.9610 Z : 1.280 + j3.4340	
Line Section 3 (OW2,O1)	OV 4.8 kV	Box DG 4.8 kV	4.0	P : 0.9927 + j1.1478 Z : 0.9927 + j1.1478	P : 0.9927 + j1.1478 Z : 0.9927 + j1.1478

Note: P and Z are positive- and zero-sequence impedances, respectively.

5.2.2 Input Data and Steady-State Condition

The time-domain model is used to simulate short-circuit faults in Scenarios OW1, OW2, and O1. Before the fault, Box Farm and the energy storage systems at OV and WF are operating at steady-state. The load demand and the power output of Microgrid OW are shown in Table 5.11 and Table 5.12 whereas Table 5.13 and Table 5.14 show the load demand and power output of Microgrid O.

Table 5.11: Pre-fault Load Consumption (Microgrid OW).

OV		WF	
P (MW)	Q (Mvar)	P (MW)	Q (Mvar)
0.7020	0.2818	0.8819	0.4937

Table 5.12: Pre-fault DG and Energy Storage Outputs (Microgrid OW).

Box Farm		Energy Storage (OV)		Energy Storage (WF)	
P (MW)	Q (Mvar)	P (MW)	Q (Mvar)	P (MW)	Q (Mvar)
0.4123	-0.1308	0.3391	0.4611	0.8634	0.4950

Table 5.13: Pre-fault Load Demand (Microgrid O).

OV	
P (MW)	Q (Mvar)
0.7020	0.2818

Table 5.14: Pre-fault DG Outputs (Microgrid O).

Box Farm		Energy Storage (OV)	
P (MW)	Q (Mvar)	P (MW)	Q (Mvar)
0.4122	-0.1308	0.3208	0.4624

A line-to-line fault is applied at $t_f = 0.5$ s. The current waveforms of the faulted phases are illustrated in Figure 5.13. It is assumed in the simulation that Box Farm will trip at $t_f + 5$ cycles. The during-fault measurements used in the methods are taken approximately three cycles after the fault is applied due to the DC offset in the fault current.

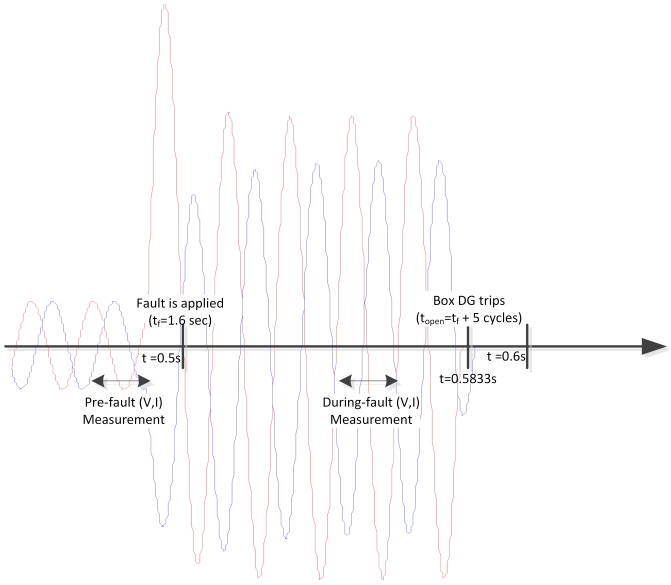

Figure 5.13: Pre-Fault, During-Fault Measurements, and Breaker Operation.

When a fault is applied, energy storage systems are disconnected from

the circuit without delay leaving Box Farm as the only possible source of fault current. This is to simulate energy storage behavior for contributing very little or no fault currents. One-ended methods are implemented for all scenarios using measurements from R173 and PQ48B. Table 5.15 lists the location of the measurements providing fault event data for each evaluation scenario.

Table 5.15: Measurement Locations.

Scenario	Simple Reactance	Takagi	Novosel
OW1	R173	R173	R173
OW2	PQ48B	PQ48B	PQ48B
O1	PQ48B	PQ48B	PQ48B

5.2.3 Evaluation of Fault Locating Methods in Microgrid OW: Scenario OW1

A line-to-line fault is applied at three different locations on Line Section 2 with a fault resistance of 0 and 5 ohms. The pre-fault current flowing through Line Section 2 is about 0.30 A and the fault current recorded by R173 is about 24 A to 30 A depending on the location of the fault. One-ended methods are implemented using fault event waveforms captured by R173. Note that measurements from R122 are not available because the recloser tripped to form the OV-WF microgrid. Results of location estimates along with their errors are shown in Table 5.16. The example current and voltage waveforms for Scenario OW1 are shown in Figure 5.14.

Microgrid OW effectively operates as two independent microgrids con-

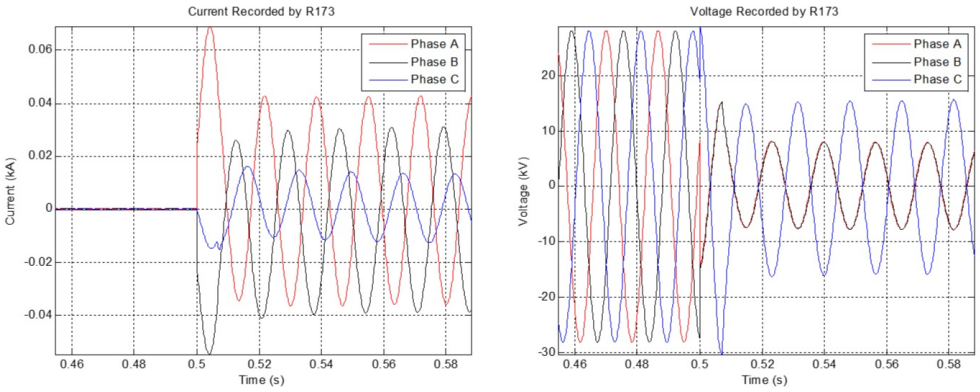

Figure 5.14: Current and Voltage Waveforms Recorded by R173 for Scenario OW1.

Table 5.16: Application of Fault Locating Methods in Scenario OW1

	Actual Location (1.90 mi.)		Actual Location (4.84 mi.)		Actual Location (6.10 mi.)	
	$R_f = 0\,\Omega$ Estimate (%Error)	$R_f = 5\,\Omega$ Estimate (%Error)	$R_f = 0\,\Omega$ Estimate (%Error)	$R_f = 5\,\Omega$ Estimate (%Error)	$R_f = 0\,\Omega$ Estimate (%Error)	$R_f = 5\,\Omega$ Estimate (%Error)
Simple Reactance	1.90 (0.00)	1.90 (0.00)	4.84 (0.00)	4.84 (0.00)	6.10 (0.00)	6.10 (0.00)
Takagi	1.90 (0.00)	1.92 (0.32)	4.84 (0.00)	4.87 (0.48)	6.10 (0.00)	6.13 (0.48)
Novosel	1.90 (0.00)	1.90 (0.00)	4.84 (0.00)	4.84 (0.00)	6.10 (0.00)	6.10 (0.00)

nected by Line Section 2 because the prefault load current flowing through it is very small. The OV load is entirely supplied by the Box Farm DG and the OV energy storage system. Likewise the WF load is also entirely supplied by its local energy storage system at WF. As a result, both load and fault currents flowing through Line Section 2 are negligible, i.e., 0.3 and 30 A, respectively. Despite this condition, fault locating methods work well because the fault current is much larger than the load current. It should be noted

that an assumption has been made that proper coordination of overcurrent protection is already in place in Microgrid OW allowing R173 to operate on line-to-line faults in Line Section 2. The error due to remote infeed does not affect the accuracy because the WN wind farm is not operational in the microgrid setting and the energy storage at WF does not contribute to fault current. All three one-ended methods are accurate to within 0.48% error as seen in Figure 5.15.

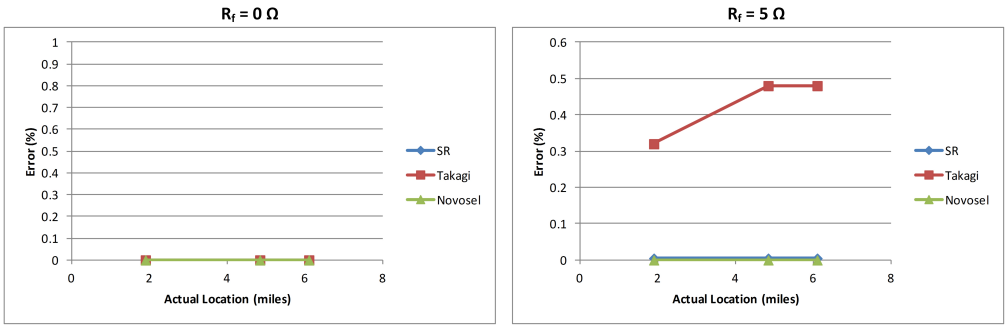

Figure 5.15: Errors in Location Estimates for Scenario OW1.

5.2.4 Evaluation of Fault Locating Methods in Microgrid OW: Scenario OW2

A line-to-line fault is simulated at two different locations on Line Section 3 with fault resistance of 0 ohms and 5 ohms. The pre-fault current flowing through Line Section 3 is about 50 A and the fault current recorded by PQ48B is about 200 A to 350 A depending on the location of the fault. Unlike Scenario G3 from Section 3.1.3 where both ends of the line contributed fault current, only Box Farm is operational in this scenario. Therefore, the

one-ended methods from PQ48B are applicable. The results are found in Table 5.17. The example current and voltage waveforms for Scenario OW2 are shown in Figure 5.16.

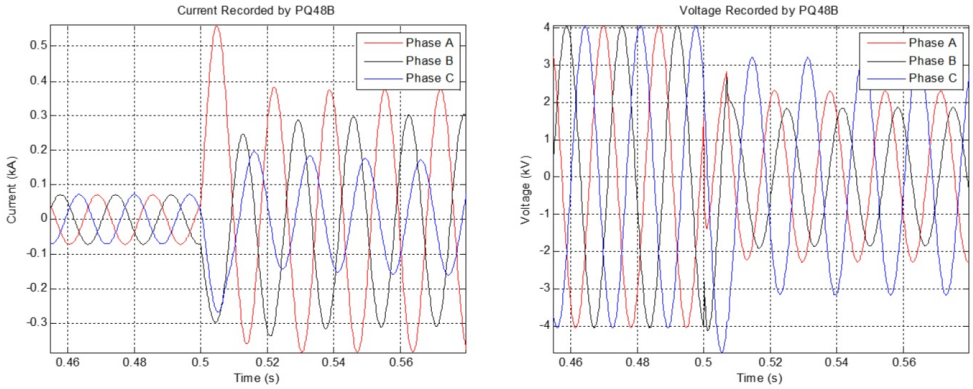

Figure 5.16: Current and Voltage Waveforms Recorded by PQ48B for Scenario OW2.

Table 5.17: Application of Fault Locating Methods in Scenario OW2

	Actual Location (0.80 mi.)		Actual Location (2.67 mi.)	
	$R_f = 0\ \Omega$ Estimate (%Error)	$R_f = 5\ \Omega$ Estimate (%Error)	$R_f = 0\ \Omega$ Estimate (%Error)	$R_f = 5\ \Omega$ Estimate (%Error)
Simple Reactance	0.80 (0.00)	0.93 (3.25)	2.67 (0.00)	2.81 (3.50)
Takagi	0.80 (0.00)	1.18 (9.50)	2.67 (0.00)	3.12 (11.25)
Novosel	0.80 (0.00)	0.96 (4.00)	2.67 (0.00)	2.83 (4.00)

As in Scenario G3 from Section 5.1.5 , the Takagi method is less accurate than the simple reactance method. This is because the Takagi method is based on an assumption that the pre-fault load current remains the same before and during the fault. However, the actual load current drawn by the OV

load differs from the pre-fault load current and as a result the Takagi method fails to give an accurate location estimate. As in Scenario OW1, WN wind farm is not operational in the microgrid setting and the energy storage systems do not contribute any fault current. Error due to remote infeed can therefore be considered negligible. The simple reactance method and the Novosel et al. method are more accurate than the Takagi method.

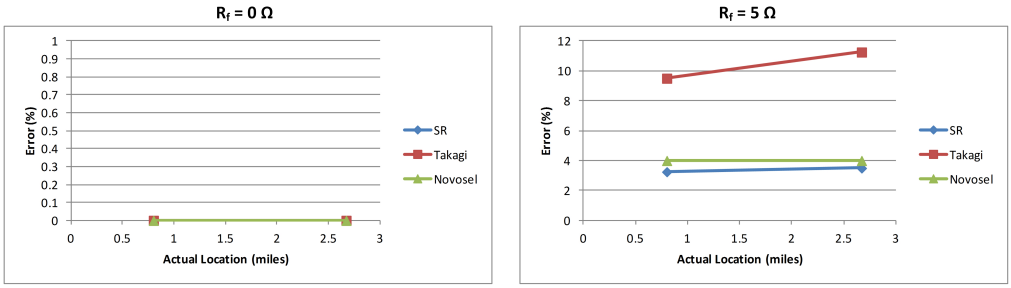

Figure 5.17: Errors in Location Estimates for Scenario OW2.

5.2.5 Evaluation of Fault Locating Methods in Microgrid O: Scenario O1

A line-to-line fault is simulated at two different locations on Line Section 3 with fault resistance of 0 ohms and 5 ohms. The pre-fault current flowing through Line Section 3 is about 50 A and the fault current recorded by PQ48B is about 200 A to 350 A depending on the location of the fault. This scenario differs from Scenario OW2 in that OV microgrid is operating alone. The one-ended methods are implemented using data from PQ48B and the results are found in Table 5.18. The current and voltage waveforms are similar to those shown in Figure 5.16.

Table 5.18: Application of Fault Locating Methods in Scenario O1

	Actual Location (0.80 mi.)		Actual Location (2.67 mi.)	
	$R_f = 0\ \Omega$ Estimate (%Error)	$R_f = 5\ \Omega$ Estimate (%Error)	$R_f = 0\ \Omega$ Estimate (%Error)	$R_f = 5\ \Omega$ Estimate (%Error)
Simple Reactance	0.80 (0.00)	0.86 (1.5)	2.67 (0.00)	2.73 (1.50)
Takagi	0.80 (0.00)	1.13 (8.25)	2.67 (0.00)	3.08 (10.25)
Novosel	0.80 (0.00)	0.89 (2.25)	2.67 (0.00)	2.76 (2.25)

In the previous scenarios the current flowing through Line Section 2 was negligible. Therefore, disconnecting Line Section 2 and isolating the OV microgrid does not have a significant impact on fault locating on Line Section 3, as seen when comparing the results of Scenario OW2 in Figure 5.17 with Scenario O1 in Figure 5.18. However, it can be noted that the disconnection of Line Section 2 decreases the error due to system load and all methods show improved accuracy of roughly 2%.

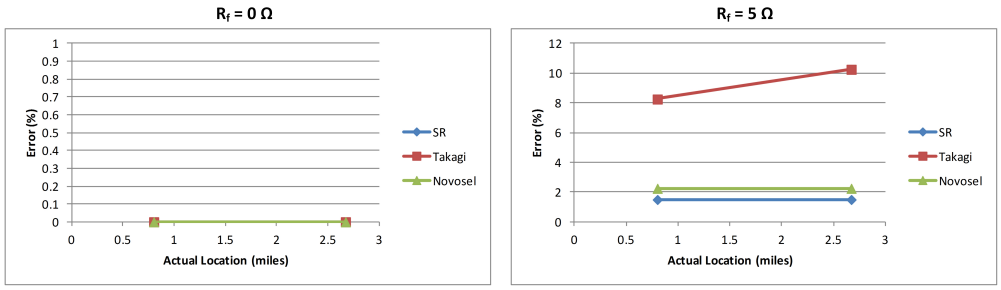

Figure 5.18: Errors in Location Estimates for Scenario O1.

Chapter 6

Implementation of Fault Locating Methods in Commercial Short-Circuit Software

The purpose of this chapter is to demonstrate the feasibility of implementing fault locating methods described in Chapter 2 in a commercial short-circuit program. Fault locating methods consisting of multiple mathematical equations are encoded as a macro embedded in the program. Any short-circuit program supporting a macro programming language can be used to implement the methods. In this Chapter, CAPE short-circuit program is used as an example program in which fault locating methods are implemented. Once a macro is defined, users can simply call the macro to determine the location estimate given by the method. This Chapter is organized as follows: CAPE Users Programming Language or CUPL is introduced in Section 6.1. Then implementing fault locating methods and their input parameters are discussed in Sections 6.2 and 6.3. Developed fault locating macros are then demonstrated in Section 6.4 and applied to actual field data in Section 6.5.

6.1 Writing Fault Locating Macros in CAPE

CAPE Users Programming Language (CUPL) is the programming language used in CAPE software. It is capable of executing arithmetic functions and logical functions. A macro consists of multiple CUPL statements. Users can define a macro using the structure in Table 6.1.

Table 6.1: Macro File Structure.

DEFINE_MACRO (macro_name,
CUPL Statement
CUPL Statement
...
)
Return

Macro is written in a text file and saved in .mac format. Macro can be executed after loading it into CAPE. CAPE provides various internal variables for the use in CUPL commands. These variables include phase voltages, line currents, and line impedances to mention just a few. Users can utilize these variables in their macro development. For example, users can access the line reactance and display its value using the following CUPL statement.

display x1_ohms from_bus to_bus circuit_number

In the above example, the location of the line is specified by defining *from_bus, to_bus*, and *circuit_number*. Tables 6.2, 6.3, and 6.4 list pre-defined

variables, mathematical functions, and if-else syntax that are frequently used in implementing fault locating methods.

Table 6.2: Line Impedance Variables.

Variables	Description
R1_PU, R1_OHMS	Line resistance (PU, ohms)
X1_PU, X1_OHMS	Line reactance (PU, ohms)
R0_PU, R0_OHMS	Line resistance (PU, ohms)
X0_PU, X0_OHMS	Line reactance (PU, ohms)

Table 6.3: Mathematical Functions.

Commands	Function
abs(A)	$\|A\|$
sqrt(A)	$sqrt(A)$
power(A,B)	A^B
cmplx(A,B)	$A + jB$
real(A)	Real part of A
aimag(A)	Imaginary part of A

Table 6.4: It-else Syntax.

IF (Boolean_expression) THEN
CUPL Statements
ELSEIF (Boolean_expression) THEN
CUPL Statements
ELSE
CUPL Statements
ENDIF

6.2 Implementation of Fault Locating Methods

The fault locating methods described in Chapter 2 are implemented using CAPE. The methods include the simple reactance, the Takagi, the Eriks-

son, and the two-ended method. The simple reactance method estimates the fault location by dividing the imaginary portion of apparent impedance by the imaginary portion of the line impedance. This method can be implemented using the following CUPL statement.

save aimag(vgU/isU)/aimag(z1_ohms) as m_simple

The variables *vgU* and *isU* are user-defined and *z1_ohms* can be accessed from the circuit model. The Takagi, the Eriksson, and the two-ended method can be implemented in a similar fashion using CUPL syntax. Three macros (*fl_one_slg*, *fl_one_ll*, and *fl_two*) are implemented. The input parameters of each macro are discussed in the following section.

6.3 Input Parameters

The input parameters are entered by the users using a graphical interface. The macro prompts the user to input the required parameters for each fault locating method. The required inputs for the macro are listed in Tables 6.5, 6.6, and 6.7. The macro prints the fault location estimates when its required parameters are entered by the user. If the required parameters are not entered, the macro simply will not print the fault locating methods that require the parameters.

The macro assumes that the measurement data are preprocessed and available in the phasor form. Symmetrical components should be calculated beforehand as well. For example, the zero-sequence current phasor should be entered separately by the user to estimate the single line-to-ground fault

location. The line impedance is read from the circuit model when the user specifies the location of the faulted branch. All the inputs will be accompanied by the directions written in the graphical pop-up interface.

Note that estimating the line-to-line fault locations requires the voltage and the current phasors from both faulted phases. For example, if line-to-line fault occurred at phase A and phase B, the voltage phasor and the current phasor from both phase A and phase B are required. Line-to-line fault locating macro can be used in estimating fault locations in three-phase faults as well. The user only needs to select any two of the three faulted phases.

Table 6.5: Input Parameters for Single Line-to-ground Faults: One-ended Methods (*fl_one_slg*).

Input	Definition
Input 1	Line Impedance
Input 2	Voltage Magnitude (LN kV)
Input 3	Voltage Angle (LN deg)
Input 4	Pre-fault Current Magnitude (kA)
Input 5	Pre-fault Current Angle (deg)
Input 6	Current Magnitude (kA)
Input 7	Current Angle (deg)
Input 8	Zero-sequence Current Magnitude (kA)
Input 9	Zero-sequence Current Angle (deg)
Input 10	Local Source Impedance (R)
Input 11	Local Source Impedance (X)
Input 12	Remote Source Impedance (R)
Input 13	Remote Source Impedance (X)

Table 6.6: Input Parameters for Line-to-line (A-B) Faults: One-ended Methods (*fl_one_ll*).

Input	Definition	Note
Input 1	Line Impedance	
Input 2	Voltage Magnitude (LN kV)	Phase A
Input 3	Voltage Angle (LN deg)	Phase A
Input 4	Voltage Magnitude (LN kV)	Phase B
Input 5	Voltage Angle (LN deg)	Phase B
Input 6	Pre-fault Current Magnitude (kA)	Phase A
Input 7	Pre-fault Current Angle (deg)	Phase A
Input 8	Pre-fault Current Magnitude (kA)	Phase B
Input 9	Pre-fault Current Angle (deg)	Phase B
Input 10	Current Magnitude (kA)	Phase A
Input 11	Current Angle (deg)	Phase A
Input 12	Current Magnitude (kA)	Phase B
Input 13	Current Angle (deg)	Phase B
Input 14	Local Source Impedance (R)	
Input 15	Local Source Impedance (X)	
Input 16	Remote Source Impedance (R)	
Input 17	Remote Source Impedance (X)	

Table 6.7: Input Parameters: Two-ended Method (*fl_two*).

Input	Definition
Input 1	Line Impedance
Input 2	Local Voltage Magnitude (LN kV)
Input 3	Local Voltage Angle (LN deg)
Input 4	Remote Voltage Magnitude (LN kV)
Input 5	Remote Voltage Angle (LN deg)
Input 6	Local Current Magnitude (kA)
Input 7	Local Current Angle (deg)
Input 8	Remote Current Magnitude (kA)
Input 9	Remote Current Angle (deg)

6.4 Demonstration Using CAPE Test System

The macros implemented are demonstrated using CAPE Test System, i.e., cape.gdb. Input data measurements are taken from a fault simulation

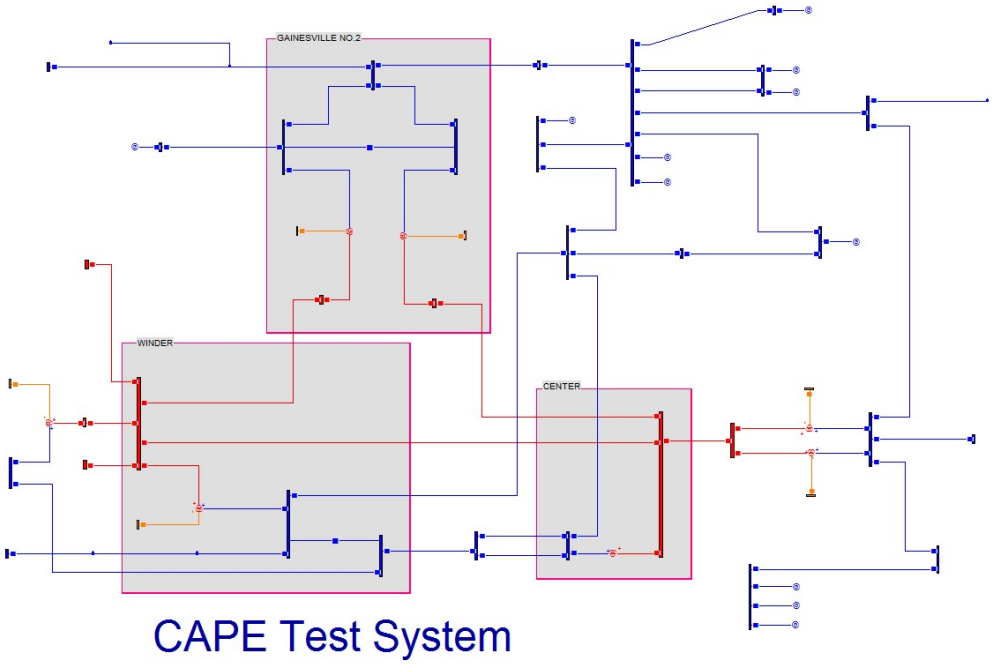

Figure 6.1: CAPE Test System.

at 0.2 pu distance with fault resistance of 5 ohms between bus 183 of Winder substation and bus 177 of Center substation. The macro is demonstrated using three steps, loading the macro, executing the macro, and entering the input variables.

1. Loading the Macro

   A user-defined macro must be loaded into CAPE before using it. This is done in File menu (File – Input File– Open File Dialog).

2. Executing the Macro

   Execute the macro by typing the macro name in the command line. Three macros (*fl_one_slg, fl_one_ll, fl_two*) are developed. The user

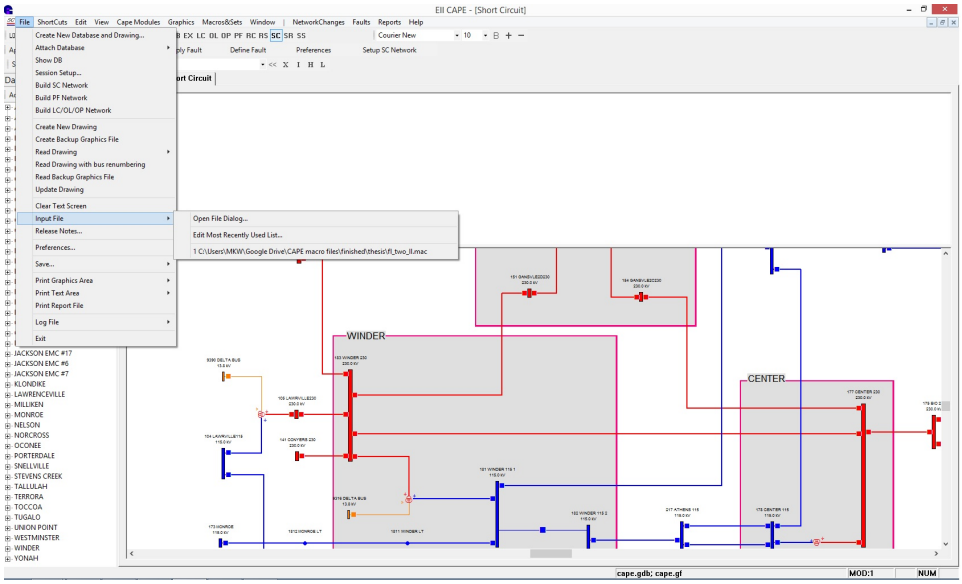

Figure 6.2: Loading the Macro.

should choose the appropriate macro depending on the fault type (single line-to-ground or line-to-line), and the availability of the measurements (one-ended or two-ended).

3. Input Variables

   The pop-up windows will prompt the user to enter necessary inputs. The user then enters the input variables as listed in Tables 6.5, 6.6, and 6.7. Examples of entering line impedance, the voltage phasor, and equivalent source impedance (R and X) are shown in Figures 6.3, 6.4, and 6.5.

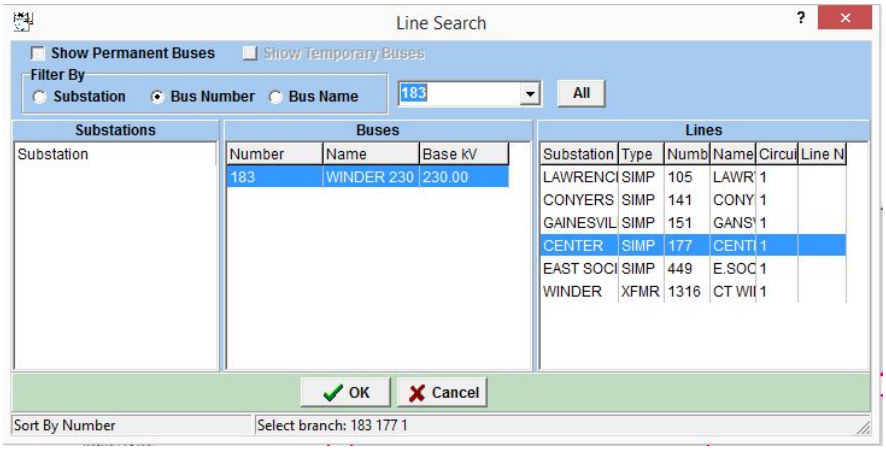

Figure 6.3: Line Impedance from Circuit Model.

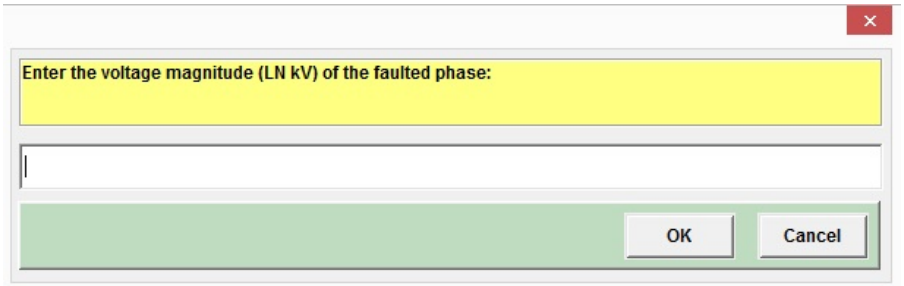

(a)

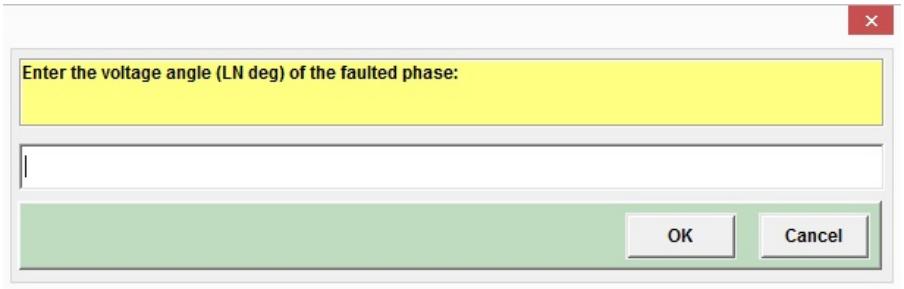

(b)

Figure 6.4: Phasor Input Example (a) Voltage Magnitude and (b) Voltage Angle.

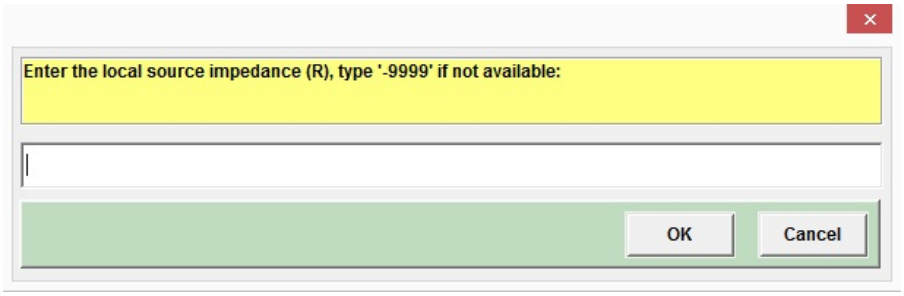

(a)

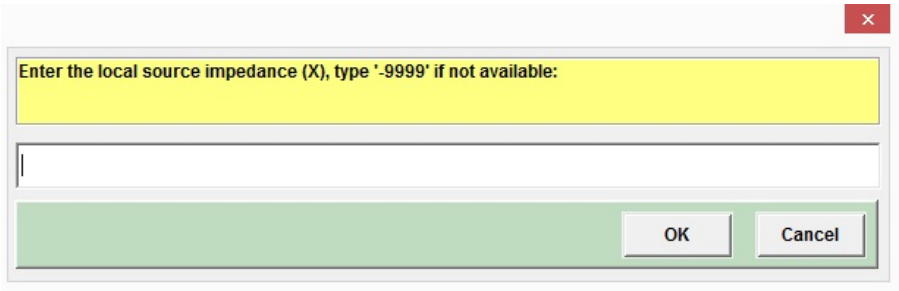

(b)

Figure 6.5: Equivalent Source Impedance Example (a) Resistance (R) and (b) Reactance (X).

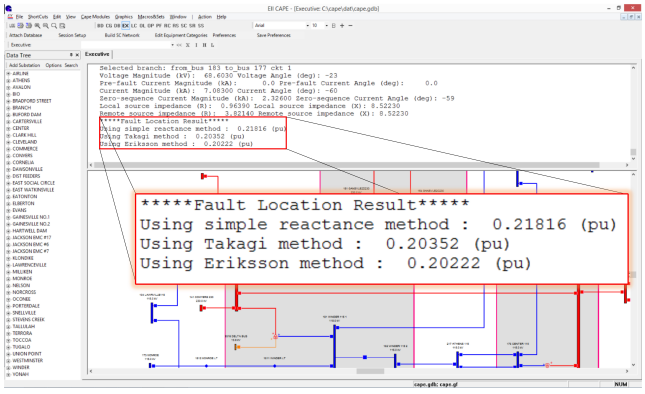

Figure 6.6: Fault Location Estimates Using *fl_one_slg*.

Table 6.8: Fault Location Estimates Using the Macros.

Macro	Fault Type	Actual Location (pu)	Estimated Location (pu)			
			Simple Reactance	Takagi	Eriksson	Negative-sequence
fl_one_slg	Single Line-to-ground	0.20	0.21816	0.20352	0.20222	N/A
fl_one_ll	Line-to-line		0.20472	0.20472	0.20368	N/A
fl_two	Single Line-to-ground		N/A	N/A	N/A	0.19991
fl_two	Line-to-line		N/A	N/A	N/A	0.20002

Table 6.9: Input Data Used in the Demonstration (*fl_one_slg*).

Input	Definition	Value
Input 1	Line Impedance	From Circuit Model
Input 2	Voltage Magnitude (LN kV)	68.603
Input 3	Voltage Angle (LN deg)	-23
Input 4	Pre-fault Current Magnitude (kA)	0.00
Input 5	Pre-fault Current Angle (deg)	0.00
Input 6	Current Magnitude (kA)	7.083
Input 7	Current Angle (deg)	-60
Input 8	Zero-sequence Current Magnitude (kA)	2.326
Input 9	Zero-sequence Current Angle (deg)	-59
Input 10	Local Source Impedance (R)	0.9639
Input 11	Local Source Impedance (X)	8.5223
Input 12	Remote Source Impedance (R)	3.8214
Input 13	Remote Source Impedance (X)	25.714

Table 6.10: Input Data Used in the Demonstration (*fl_one_ll*).

Input	Definition	Value
Input 1	Line Impedance	From Circuit Model
Input 2	Voltage Magnitude (LN kV)	95.544
Input 3	Voltage Angle (LN deg)	-34
Input 4	Voltage Magnitude (LN kV)	62.481
Input 5	Voltage Angle (LN deg)	-102
Input 6	Pre-fault Current Magnitude (kA)	0.00
Input 7	Pre-fault Current Angle (deg)	0
Input 8	Pre-fault Current Magnitude (kA)	0.00
Input 9	Pre-fault Current Angle (deg)	0
Input 10	Current Magnitude (kA)	8.873
Input 11	Current Angle (deg)	-39
Input 12	Current Magnitude (kA)	8.873
Input 13	Current Angle (deg)	141
Input 14	Local Source Impedance (R)	0.9639
Input 15	Local Source Impedance (X)	8.5223
Input 16	Remote Source Impedance (R)	3.8214
Input 17	Remote Source Impedance (X)	25.714

Table 6.11: Input Data Used in the Demonstration (*fl_two*, Single Line-to-ground Fault).

Input	Definition	Value
Input 1	Line Impedance	From Circuit Model
Input 2	Local Voltage Magnitude (LN kV)	20.402
Input 3	Local Voltage Angle (LN deg)	-156
Input 4	Remote Voltage Magnitude (LN kV)	18.651
Input 5	Remote Voltage Angle (LN deg)	-157
Input 6	Local Current Magnitude (kA)	2.379
Input 7	Local Current Angle (deg)	-60
Input 8	Remote Current Magnitude (kA)	0.717
Input 9	Remote Current Angle (deg)	-58

Table 6.12: Input Data Used in the Demonstration (*fl_two*, Line-to-line Fault).

Input	Definition	Value
Input 1	Line Impedance	From Circuit Model
Input 2	Local Voltage Magnitude (LN kV)	43.938
Input 3	Local Voltage Angle (LN deg)	-105
Input 4	Remote Voltage Magnitude (LN kV)	40.166
Input 5	Remote Voltage Angle (LN deg)	-106
Input 6	Local Current Magnitude (kA)	5.123
Input 7	Local Current Angle (deg)	-9
Input 8	Remote Current Magnitude (kA)	1.545
Input 9	Remote Current Angle (deg)	-7

6.5 Macro Application to Actual Field Data

The macros implemented are applied to two fault event data files. Each event file consists of two fault clearing operations. Voltage and current waveforms of the events are shown in Figure 6.7 and Figure 6.8. Since the events are single line-to-ground faults with measurements from one end, the macro *fl_one_slg* is executed to estimate the fault location.

The four parts of the field data are taken separately and preprocessed to provide voltage and current inputs in the phasor form. The line impedance is captured from the circuit model available in CAPE. The error estimates of the macro cannot be quantified because the actual fault location is not available. However, the location estimates of all four parts give similar results, implying that the results given by the macro are reasonable.

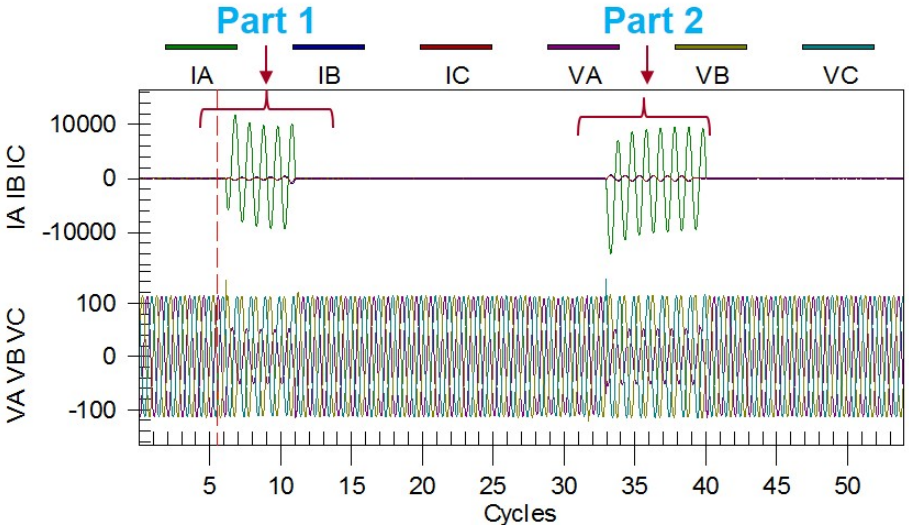

Figure 6.7: Event 1: A-G Fault, 1/1/13, 09:38:33.94.

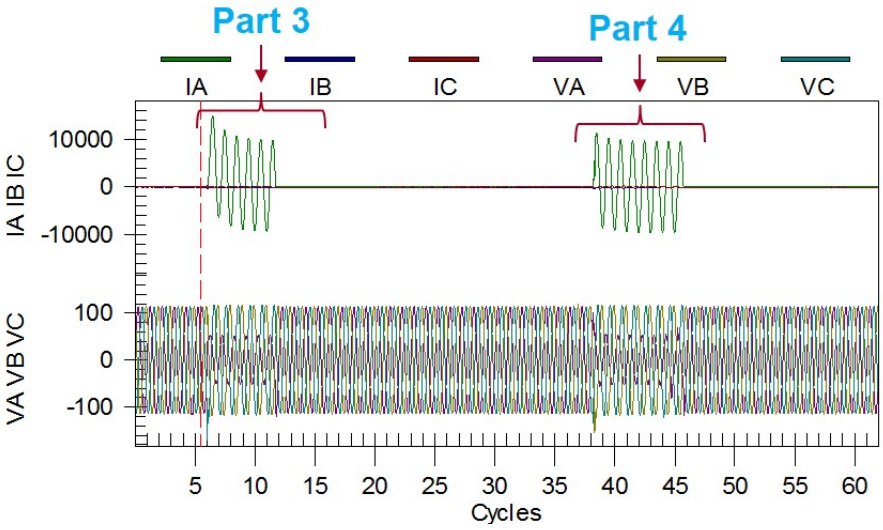

Figure 6.8: Event 2: A-G Fault, 1/1/13, 09:42:23.08.

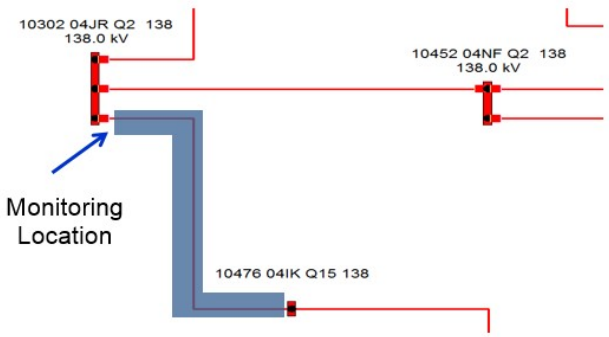

Figure 6.9: Circuit Model in CAPE.

Table 6.13: Input Data for the Fault Events.

Input	Value			
	Event 1		Event 2	
	Part 1	Part 2	Part 3	Part 4
Input 1	From Circuit Model	From Circuit Model	From Circuit Model	From Circuit Model
Input 2	35.9050	36.1817	36.1302	36.3446
Input 3	171.99	157.51	-14.86	-24.64
Input 4	0.0214	0.0002	0.0004	0.0002
Input 5	-157.29	52.18	-156.39	-172.23
Input 6	6.6964	6.9236	6.9101	6.8006
Input 7	97.32	83.90	-91.39	-99.89
Input 8	2.1102	2.0718	2.3026	2.2635
Input 9	96.88	84.12	-97.37	-99.83
Input 10	0.7186	0.5256	0.5426	0.5647
Input 11	6.3416	5.5797	5.5981	5.6768
Input 12	1.1819	1.1819	1.1819	1.1819
Input 13	9.4331	9.4331	9.4331	9.4331

Table 6.14: Location Estimates Using the Macro.

Event 1&2	Actual Location (pu)	Estimated Location (pu)		
		Simple Reactance	Takagi	Eriksson
Part 1	Unknown	0.54313	0.54241	0.54241
Part 2		0.53663	0.53498	0.53485
Part 3		0.52729	0.53085	0.53099
Part 4		0.53073	0.53039	0.53037

Chapter 7

Conclusion

This thesis presents applications of impedance-based fault locating methods in power systems. Chapter 2 introduces representative fault locating methods while in Chapter 3, the DC offsets that are present in the fault current waveforms are removed as they affect the magnitude response at the fundamental frequency. The approach presented is applied to the first few cycles of asymmetrical fault current waveforms and the resulting fault location estimates are found to be more robust.

In Chapter 4, a distribution system interconnected to distributed generation is considered. It is shown that when a fault occurs upstream from the distribution generation, the accuracy of the fault location estimates are affected by the load served downstream from the DG. A virtual monitor placed at the POI is used to improve the fault location estimates by providing the remote equivalent source impedance for the Eriksson method, and the remote measurements for the two-ended methods.

In Chapter 5, the fault locating methods are applied to distribution circuits with distributed generation operating in grid-interconnected and microgrid modes. For each operating mode, the fault location estimated by the

methods are evaluated. In Chapter 6, the fault locating methods are implemented using macro programming provided in CAPE software. The graphical interfaces assist the users in entering the required inputs needed for the fault location methods.

Bibliography

[1] P. Wheeler, J. Rodriguez, J. Clare, L. Empringham, and A. Weinstein, "IEEE guide for determining fault location on AC transmission and distribution lines," *IEEE Std C37.114-2004*, pp. 1–36, 2005.

[2] K. Zimmerman and D. Costello, "Impedance-based fault location experience," in *Protective Relay Engineers, 2005 58th Annual Conference for*, pp. 211–226, 2005.

[3] T. Takagi, Y. Yamakoshi, M. Yamaura, R. Kondow, and T. Matsushima, "Development of a new type fault locator using the one-terminal voltage and current data," *Power Apparatus and Systems, IEEE Transactions on*, vol. PAS-101, no. 8, pp. 2892–2898, 1982.

[4] L. Eriksson, M. Saha, and G. D. Rockefeller, "An accurate fault locator with compensation for apparent reactance in the fault resistance resulting from remore-end infeed," *Power Apparatus and Systems, IEEE Transactions on*, vol. PAS-104, no. 2, pp. 423–436, 1985.

[5] D. Novosel, D. Hart, E. Udren, and J. Garitty, "Unsynchronized two-terminal fault location estimation," *Power Delivery, IEEE Transactions on*, vol. 11, no. 1, pp. 130–138, 1996.

[6] E. Schweitzer, "Evaluation and development of transmission line fault-locating techniques which use sinusoidal steady-state information," *Computers & Electrical Engineering*, vol. 10, no. 4, pp. 269 – 278, 1983.

[7] M. Saha, J. Izykowski, and E. Rosolowski, *Fault Location on Power Networks*. Springer, 2010.

[8] M. Sachdev and M. A. Baribeau, "A new algorithm for digital impedance relays," *Power Apparatus and Systems, IEEE Transactions on*, vol. PAS-98, pp. 2232–2240, Nov 1979.

[9] G. Benmouyal, "Removal of DC-offset in current waveforms using digital mimic filtering," *Power Delivery, IEEE Transactions on*, vol. 10, pp. 621–630, Apr 1995.

[10] J. Nunes and A. Bretas, "A impedance-based fault location technique for unbalanced distributed generation systems," in *PowerTech, 2011 IEEE Trondheim*, pp. 1–7, 2011.

[11] C. Orozco-Henao, J. Mora-Florez, and S. Perez-Londono, "A robust method for single phase fault location considering distributed generation and current compensation," in *Transmission and Distribution: Latin America Conference and Exposition (T D-LA), 2012 Sixth IEEE/PES*, pp. 1–7, 2012.

[12] J. Marvik, H. Hoidalen, and A. Petterteig, *Evaluation of simple fault location on a MV feeder with DG, using fundamental frequency components.*

NORDAC, 2008.

[13] T. Short, *Electric Power Distribution Handbook*. CRC Press, 2003.

[14] EPRI, *Distributed generation modeling guidelines*. Palo Alto, CA.

[15] T. H. M. EL-Fouly and C. Abbey, "On the compatibility of fault location approaches and distributed generation," in *Integration of Wide-Scale Renewable Resources Into the Power Delivery System, 2009 CIGRE/IEEE PES Joint Symposium*, pp. 1–5, 2009.